moment whether this can be explained by configuration interaction and hybridization effects or whether it indicates an overlap of the top occupied Pt d band (probably d_z^2) with an s-p band.

[1]K. Krogmann, Angew. Chem. (Int. Ed. Engl.) 8, 35 (1968).
[2]D. Kuse and H. R. Zeller, Phys. Rev. Lett. 27, 1060 (1971); H. P. Geserich, H. D. Hausen, K. Krogmann, and P. Stampfl, Phys. Status Solidi A 10, 537 (1972); P. Brüesch and F. Lehmann, Solid State Commun. 10, 579 (1972).
[3]J. Bernasconi, P. Brüesch, D. Kuse, and H. R. Zeller (unpublished).
[4]A. S. Berenblyum, L. I. Buravov, M. D. Khidekel, I. F. Shchegolev, and E. B. Yakimov, Zh. Eksp. Teor. Fiz. Pis'ma Red. 13, 619 (1971) [JETP Lett. 13, 440 (1971)].
[5]M. J. Rice and J. Bernasconi, J. Phys. F 2, 902 (1972).
[6]M. J. Rice and J. Bernasconi, J. Phys. F 3, 55 (1973).
[7]J. Bernasconi, D. Kuse, M. J. Rice, and H. R. Zeller, J. Phys. C 5, L 127 (1972).
[8]A. N. Bloch, R. B. Weisman, and C. M. Verma, Phys. Rev. Lett. 28, 753 (1972).
[9]N. F. Mott and W. D. Twose, Adv. Phys. 10, 107 (1961); R. E. Borland, Proc. Phys. Soc. Lond. 78, 926 (1961).
[10]M. J. Rice, Phys. Lett. A 39, 289 (1972).
[11]R. E. Peierls, *Quantum Theory of Solids* (Oxford U. P., London, 1955).
[12]R. Comes, M. Lambert, H. Launois, and H. R. Zeller (unpublished).
[13]A. J. Epstein, S. Etemad, A. F. Garito, and A. J. Heeger, Phys. Rev. B 5, 952 (1972).
[14]W. Rüegg, Helv. Phys. Acta (to be published).
[15]D. Walcher, Z. Phys. 246, 123 (1971).
[16]D. Agresti, E. Kankeleit, and B. Person, Phys. Rev. 155, 1339 (1967).
[17]U. Raff, K. Alder, and G. Bauer, Helv. Phys. Acta 45, 427 (1972).

PHYSICAL REVIEW B VOLUME 8, NUMBER 3 1 AUGUST 1973

Optical Spectra of Cr^{3+} Pairs in the Spinel $ZnGa_2O_4$

G. G. P. van Gorkom, J. C. M. Henning, and R. P. van Stapele
Philips Research Laboratories, Eindhoven, The Netherlands
(Received 5 February 1973)

Exchange interactions of nearest-neighbor Cr^{3+} pairs in $ZnGa_2O_4$ have been studied in detail. An analysis of the emission, absorption, and luminescence excitation spectra yield the ($^4A_2$, $^4A_2$) ground-state level splittings and the ($^4A_2$, ^2E) excited-state splittings. The first are described by $-J\vec{S}_1\cdot\vec{S}_2+j(\vec{S}_1\cdot\vec{S}_2)^2$, with $S_1=S_2=3/2$, $J=-22.2\pm0.5$ cm^{-1}, and $j=-1.7\pm0.3$ cm^{-1}. The ($^4A_2$, ^2E) level splittings are compared with the values calculated from the orbital-dependent exchange Hamiltonian $\mathcal{H}_{ex}=-\sum_{ij}J_{ij}\vec{s}_i\cdot\vec{s}_j$, where $s_i=s_j=1/2$ and the sum is over the t_{2g} orbitals of the Cr^{3+} ion. In the local C_{2v} symmetry of the pair, there are four independent J_{ij} parameters which have been determined as $J_c=+39$ cm^{-1}, $J_c'=+117$ cm^{-1}, $J_d=-561$ cm^{-1}, and $J_\pi=-105$ cm^{-1}. The large value of J_d is a consequence of the direct overlap between $t_2\zeta$ functions, which is possible in the 90° exchange configuration of nearest-neighbor Cr pairs in the spinel structure. The relative intensities of the different pair lines are compared with values calculated from the mechanism of the exchange-induced dipole moment and reasonable agreement is found.

I. INTRODUCTION

Trivalent chromium ions have a strong preference for an octahedral surrounding. In many chromium compounds the octahedra occupied by Cr^{3+} share an edge (Fig. 1). In such compounds the nearest-neighbor exchange interaction is a so-called 90° superexchange between two chromium ions. Among the superexchange interactions this interaction has for long attracted the attention. In compounds with a small lattice parameter like $LiCrO_2$, where the Cr-Cr distance is 2.88 Å, the asymptotic Curie temperature Θ_C is large and negative ($\Theta_C=-577$ °K),[1] but in compounds with Cr-Cr distance larger than some 3.5 Å the asymptotic Curie temperature is positive[2-6] (Fig. 2). It is among such Cr compounds with large lattice parameter that one finds the well-known semiconducting ferromagnets $CdCr_2S_4$ and $CdCr_2Se_4$.[5,7]

The explanation of this marked dependence on the distance of the chromium ions was based on (i) positive exchange between electrons in t_{2g} orbits which have a zero overlap because of symmetry (e.g., between xz on A and xz or xy on B in Fig. 1), and (ii) negative exchange between electrons in t_{2g} orbits which have a nonzero overlap (e.g., xy on A and xy on B or between xz on A and yz on B). The signs of these interactions follow from the Kanamori-Goodenough rules,[8,9] which are in qualitative accordance with Anderson's theory of superexchange interactions.[10] Among the negative interactions the $(xy)_A$-$(xy)_B$ interaction is assumed to be

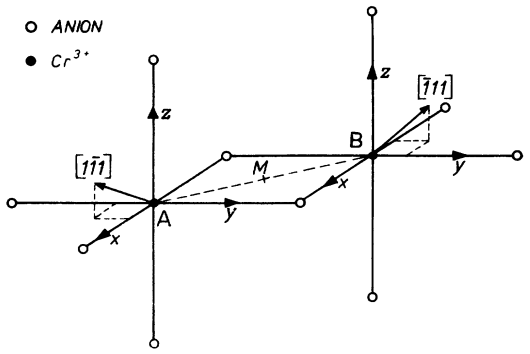

FIG. 1. Local symmetry of a nearest-neighbor Cr^{3+} pair in spinel. The Cr^{3+} ions occupy the octahedral sites. The local trigonal symmetry axes are indicated by arrows. A and B denote Cr^{3+} ion *A* and Cr^{3+} ion *B*, respectively (and not the so-called *A* and *B* sites).

the dominant one at short distances by virtue of a direct overlap of the $t_{2g}(3d)$ wave functions.[11,12] The direct overlap will decrease strongly with increasing separation of the chromium ions, which explains the observed steep increase of Θ_C with increasing lattice parameter. The balance of the other interactions in compounds with a large lattice parameter is apparently such that positive Θ_C's result.

In striking contrast with the picture sketched above, Blazey[13] observed positive nearest-neighbor interactions between Cr^{3+} ions in $ZnAl_{2-x}Cr_xO_4$. He deduced the sign and the magnitude of the exchange interaction from a Landé sequence of luminescence lines close to the $^2E \rightarrow {}^4A_2$ lines of single Cr^{3+} ions, which were attributed to pairs of Cr ions. However, Wood *et al.*[14] questioned the assignment of these lines. Not all the lines of the Landé sequence were present in their fluorescence spectrum of $ZnAl_2O_4$ doped with Cr.

In view of these contradictions it is of importance to investigate exchange-coupled Cr pairs in a diamagnetic spinel lattice in greater detail. Since it is known[15] that not only the distance between the Cr ions but also the Cr-O-Cr bond angle determines the strength of the exchange, $ZnGa_2O_4$ is a very suitable host lattice: Both the lattice parameter ($a = 8.330$ Å) and the u parameter ($u = 0.38675$)[16] are very close to that of $ZnCr_2O_4$ ($a = 8.327$ Å and $u = 0.385$).[4] One of us[17-19] started the investigation of Cr pairs in this lattice with ESR experiments. In this paper we present the results of a study of the 90° exchange between Cr ions in $ZnGa_2O_4$ by means of optical spectroscopy.

In Sec. II we describe the crystal structure of $ZnGa_2O_4$, sample preparation, and experimental setup. In Sec. III, the theory of the exchange-coupled Cr^{3+} ion pairs in the spinel structure is given. Luminescence, absorption, and excitation measurements are described in Sec. IV. Thereafter, in Sec. V, a comparison between experiment and theory is made from which the exchange parameters are deduced. Finally, the results are discussed in Sec. VI.

II. CRYSTAL STRUCTURE, SAMPLE PREPARATION, AND EXPERIMENTAL SETUP

The unit cell of compounds with spinel structure belongs to the cubic space group O_h^7 ($Fd3m$) and contains eight formula units. There are two types of metal ion sites: the *A* site has tetrahedral coordination (point group T_d) and the *B* site has sixfold-distorted octahedral coordination (D_{3d} symmetry). In $ZnGa_2O_4:Cr^{3+}$ the Zn^{2+} ions occupy *A* sites, the Ga^{3+} and the Cr^{3+} the *B* sites. In this paper we are concerned with nearest-neighbor pairs of Cr^{3+} ions. The local trigonal axes of the Cr^{3+} ions of this pair are not parallel but include an angle of about 110° with each other. The local environment of the Cr^{3+} pair is sketched in Fig. 1. It can be seen that the symmetry of the pair is C_{2v} (which means that the point group of the point *M* midway between the Cr^{3+} ions is C_{2v}). The distance between the Cr^{3+} ions of the nearest-neighbor pair is 2.945 Å; for second- and third-neighbor pairs the distances are 5.101 and 5.890 Å, respectively.

The samples used in this study were single crystals and powders $ZnGa_{2-x}Cr_xO_4$. The single crystals were grown by a method described earlier[20]; the powders were produced by a solid-state reaction of ZnO, Ga_2O_3, and the desired amount of

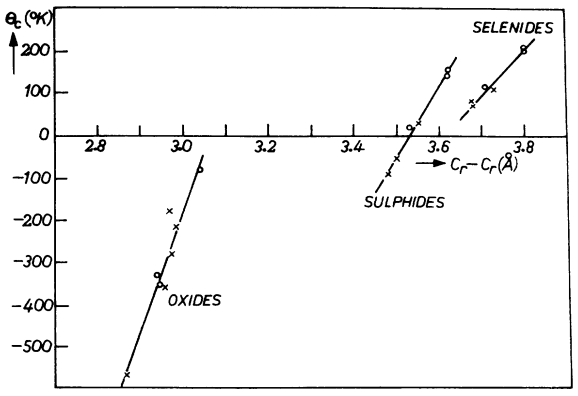

FIG. 2. Asymptotic Curie temperature Θ_C of compounds with a nearest-neighbor Cr^{3+}-anion-Cr^{3+} angle of about 90° as a function of the Cr^{3+}-Cr^{3+} distance. Each point in the figure represents a specific compound, which is listed (with references to the original papers) in Ref. 15. We remark that in the series oxides the Cr-O distance is nearly a constant (about 1.99 Å) and the increasing Cr-Cr distance is caused by the increase of the Cr-anion-Cr angle. In the figure the circles denote compounds with normal spinel structure, the crosses compounds with other structures (see Ref. 15).

Cr_2O_3. This resulted in powders $ZnGa_{2-x}Cr_xO_4$ with x ranging from 0.0015 to 0.06. The amount of chromium was determined photometrically with diphenylcarbazide with an accuracy of 5%.

Emission spectra were recorded by standard optical techniques. The Cr^{3+} luminescence was excited by pumping in the ultraviolet, blue, or green absoprtion bands with a mercury lamp or sometimes with an Ar^+-ion laser operating at 5145 Å. The luminescence light is analyzed using a $\frac{1}{2}$-m Jarrell-Ash monochromator (resolution about 2 Å) and a cooled photomultiplier (EMI 9659 B of Philips XP1003). Luminescence decay times were measured as follows. The luminescence is excited by the chopped light of a CS-200 mercury lamp, filtered by suitable filters. The emitted light is fed into a small monochromator to isolate the desired emission line and then detected with a cooled XP1003 ($S20$) photomultiplier; the photocurrent is fed into a Waveform Eductor and then displayed on an oscilloscope. The fall-off time of the exciting light pulse is about 400 μsec, so the determined decay times have about this accuracy. A number of lines (partly) overlap, and so the accuracy may then be less. Moreover, most of the lines studied did not exhibit a simple exponential decay, especially in the higher-doped samples; in these cases a mean decay time will be given.

Absorption spectra were taken by irradiating a single crystal $ZnGa_{2-x}Cr_xO_4$ with monochromatic light and measuring the amount of transmitted light as a function of wavelength. Luminescence excitation spectra were measured as follows. Monochromatic light of variable wavelength is incident on the sample. The luminescence light leaving the sample is fed into a second monochromator tuned to the emission line of which we want to know the excitation spectrum; the light leaving the second monochromator is then detected by a photomultiplier.

In most of the experiments the sample is mounted on the cold finger of a liquid-helium cryostat. The cold finger is a block of copper in which a calibrated carbon resistor is mounted for temperature measurement. Between the sample and the liquid-helium reservoir, a heating coil and a heat resistor (a rod of copper, brass, or stainless steel) have been mounted. A regulating unit keeps the sample temperature constant within 0.2 °K of the intended temperature. With this arrangement sample temperatures in the range 4.5–200 °K were possible.

III. THEORY

A. Pair Levels of Optical Ground State

In describing the results of ESR or susceptibility measurements on exchange-coupled pairs of magnetic ions, the phenomenological exchange Hamiltonian

$$\mathcal{H}_{ex} = -J\vec{S}_1 \cdot \vec{S}_2 + j(\vec{S}_1 \cdot \vec{S}_2)^2 \tag{1}$$

is frequently used, sometimes extended with anisotropic terms which can be neglected for the description of the optical spectra of Cr^{3+} pairs in $ZnGa_2O_4$ because they are too small. In (1), J and j are, respectively, the isotropic bilinear and the biquadratic exchange parameters; $\vec{S}_1$ and $\vec{S}_2$ are the ionic spins of ion 1 and ion 2, respectively.

The exchange Hamiltonian (1) commutes with the total spin $\vec{S}$ of the pair, and so the energy levels can be classified with the possible eigenvalues of $\vec{S}$. For Cr^{3+} ion pairs we have $S_1 = S_2 = \frac{3}{2}$ and the exchange Hamiltonian (1) gives rise to four levels with energy E:

$$\begin{aligned} &S=0\,, \quad E=+\tfrac{15}{4}J+\tfrac{225}{16}j\,,\\ &S=1\,, \quad E=+\tfrac{11}{4}J+\tfrac{121}{16}j\,,\\ &S=2\,, \quad E=+\tfrac{3}{4}J+\tfrac{9}{16}j\,,\\ &S=3\,, \quad E=-\tfrac{9}{4}J+\tfrac{81}{16}j\,. \end{aligned} \tag{2}$$

Although (1) can be used to give a correct description of the ground state of a Cr^{3+} pair ($^4A_2$, $^4A_2$), this is not the case when one of the ions of the pair is in the ^2E state because of the orbital degeneracy of this state. This is the reason why early attempts of Clogston[21] and Nikiforov *et al.*[22] failed in explaining the structure of the first-excited state of Cr^{3+} pairs in ruby.

In Sec. III B we shall introduce an exchange Hamiltonian which gives a more correct description of the excited state of a pair.

B. Electronic Structure of Optically Excited ($^4A_2$,^2E) State

Following the original ideas of Van Vleck,[23] an isotropic coupling proportional to the scalar product $\vec{s}_i \cdot \vec{s}_j$ of the electrons is presumed to exist between any pair of electrons, where the coefficient is dependent on the detailed shape and orientation of the corresponding orbitals in which they move. Formally, according to Elliott and Thorpe[24] the exchange interaction may be written in terms of irreducible tensor operators formed from the orbital angular momenta. A simplification arises when interactions are considered within a multiplet or between multiplets which are built up from the same set of singly occupied orbitals. Such is the case with the ^2E and $^4A_2$ states of Cr^{3+} where we have exactly one electron in each of the three t_{2g} orbitals. Using the results of Culvahouse *et al.*[25] the exchange Hamiltonian can then be written

$$\mathcal{H}_{ex} = -\sum_{i,j} J_{ij}\vec{s}_{iA} \cdot \vec{s}_{jB}\,, \tag{3}$$

where J_{ij} is a parameter describing the exchange interaction between an electron in orbital i on ion A and an electron in orbital j on ion B; $\vec{s}_{iA}$ and $\vec{s}_{jB}$

are the spins of these electrons. Equation (3) was used by Pryce,[26] van der Ziel,[27] and Huang[28] to describe the properties of chromium pairs in Al_2O_3, $LaAlO_3$, and V^{2+} pairs in $KMgF_3$, respectively, and by Birgeneau[29] to account for energy transfer processes in ruby.

In what follows an attempt will be made to describe the splittings of the $({}^4A_2, {}^2E)$ state in terms of the interaction Hamiltonian Eq. (3). We will neglect biquadratic exchange terms, partly because of simplicity and because they are expected to be much smaller than the bilinear exchange terms.

Since the Cr^{3+} ion has three $3d$ electrons, each of which is in one t_{2g} orbital, we have generally nine J_{ij} parameters, but if the Cr^{3+} pair has a symmetry higher than C_1 then certain J_{ij}'s will be identical. As mentioned earlier, the local symmetry of the nearest-neighbor (nn) pairs in the spinel lattice is C_{2v}. Application of the symmetry operations of C_{2v} leads to four inequivalent orbital exchange parameters:

$$\begin{aligned} &J_{\xi\xi} = J_{\eta\eta} = J_c \,, \\ &J_{\xi\eta} = J_{\eta\xi} = J_\pi \,, \\ &J_{\xi\zeta} = J_{\eta\zeta} = J_{\zeta\xi} = J_{\zeta\eta} = J_c' \,, \\ &J_{\zeta\zeta} = J_d \,. \end{aligned} \tag{4}$$

Here, the three t_{2g} orbitals are denoted by $\xi \equiv |yz\rangle$, $\eta \equiv |zx\rangle$, and $\bar{\zeta} \equiv |xy\rangle$; the subscripts A and B denote the different ions have been left out; x, y, and z refer to the local Cartesian coordinates of the Cr ions (Fig. 1). These four exchange constants will be treated as empirical parameters which have to be determined from the observed pair spectra. Their physical meaning will be discussed in Sec. VI B.

Let us now consider the optical ground state of the pair to see the connection of J of Eq. (1) with the J_{ij}'s. It can easily be shown that for the ground-state equation, (1) can be used instead of (3) if we take

$$J = \tfrac{1}{9} \sum_{i,j} J_{ij} = \tfrac{1}{9} (2J_c + 4J_c' + J_d + 2J_\pi) \,. \tag{5}$$

We shall now calculate the energies of the different spin multiplets of the excited state of the nn pairs. The four substates of the single-ion ground state are given by

$$\begin{aligned} &|A(\tfrac{3}{2})\rangle = |\xi\eta\zeta| \,, \\ &|A(\tfrac{1}{2})\rangle = (1/\sqrt{3})\,(|\bar{\xi}\eta\zeta| + |\xi\bar{\eta}\zeta| + |\xi\eta\bar{\zeta}|) \,, \\ &|A(-\tfrac{1}{2})\rangle = (1/\sqrt{3})\,(|\xi\bar{\eta}\bar{\zeta}| + |\bar{\xi}\eta\bar{\zeta}| + |\bar{\xi}\bar{\eta}\zeta|) \,, \\ &|A(-\tfrac{3}{2})\rangle = |\bar{\xi}\bar{\eta}\bar{\zeta}| \,, \end{aligned} \tag{6}$$

where $|\xi\eta\bar{\zeta}|$ denotes a normalized Slater determinant for two electrons with spin up in orbitals ξ and η and one electron with spin down in ζ. The ${}^2E$ functions are given by[26]

$$\begin{aligned} &|E^+(\tfrac{1}{2})\rangle = (1/\sqrt{3})\,(\omega|\bar{\xi}\eta\zeta| + \omega^2|\xi\bar{\eta}\zeta| + |\xi\eta\bar{\zeta}|) \,, \\ &|E^-(\tfrac{1}{2})\rangle = (1/\sqrt{3})\,(\omega^2|\bar{\xi}\eta\zeta| + \omega|\xi\bar{\eta}\zeta| + |\xi\eta\bar{\zeta}|) \,, \\ &|E^+(-\tfrac{1}{2})\rangle = (-1/\sqrt{3})\,(\omega|\xi\bar{\eta}\bar{\zeta}| + \omega^2|\bar{\xi}\eta\bar{\zeta}| + |\bar{\xi}\bar{\eta}\zeta|) \,, \\ &|E^-(-\tfrac{1}{2})\rangle = (-1/\sqrt{3})\,(\omega^2|\xi\bar{\eta}\bar{\zeta}| + \omega|\bar{\xi}\eta\bar{\zeta}| + |\bar{\xi}\bar{\eta}\zeta|) \,, \end{aligned} \tag{7}$$

where $\omega = e^{2\pi i/3}$. For the present spin-orbit coupling and trigonal field are neglected.

In the singly excited pair state, when one ion is in the ${}^2E$ state and the other in the ${}^4A_2$, the exchange Hamiltonian (3) couples the spins of both ions, resulting in eight states, four having total spin $S=1$ and four with $S=2$. It is then convenient to use wave functions which are constructed from the single-ion wave functions by coupling the ionic spins of both ions, using tables of Wigner coefficients.[30] The wave functions are

$$\begin{aligned} &S=1, \; m_S=1 \,, \\ &a = \sqrt{\tfrac{3}{4}}\,|E^+(-\tfrac{1}{2}), A(\tfrac{3}{2})\rangle - \sqrt{\tfrac{1}{4}}\,|E^+(\tfrac{1}{2}), A(\tfrac{1}{2})\rangle \,, \\ &b = \sqrt{\tfrac{3}{4}}\,|E^-(-\tfrac{1}{2}), A(\tfrac{3}{2})\rangle - \sqrt{\tfrac{1}{4}}\,|E^-(\tfrac{1}{2}), A(\tfrac{1}{2})\rangle \,, \\ &c = \sqrt{\tfrac{3}{4}}\,|A(\tfrac{3}{2}), E^+(-\tfrac{1}{2})\rangle - \sqrt{\tfrac{1}{4}}\,|A(\tfrac{1}{2}), E^+(\tfrac{1}{2})\rangle \,, \\ &d = \sqrt{\tfrac{3}{4}}\,|A(\tfrac{3}{2}), E^-(-\tfrac{1}{2})\rangle - \sqrt{\tfrac{1}{4}}\,|A(\tfrac{1}{2}), E^-(\tfrac{1}{2})\rangle \,, \end{aligned} \tag{8}$$

and similar expressions for the other $S=1$, m_S and $S=2$, m_S states, which are easily derived from the tables of Wigner coefficients.[30] Using this basis, the exchange operator (3) may be represented by a different matrix for each value of the total spin S (independent of m_S). They are given by Pryce.[26] A most convenient form of the $S=1$ and $S=2$ matrices is obtained by taking combinations which are symmetric (s) or antisymmetric (as) in the ions,

$$\begin{aligned} &\text{s:} \quad a+c; \quad b+d \,, \\ &\text{as:} \quad a-c; \quad b-d \,, \end{aligned} \tag{9}$$

as basis functions.

Following Pryce[26] we define the auxiliary quantities

$$\begin{aligned} K &= -\frac{1}{18} \sum_{i,j} \omega^{-i+j} J_{ij} \,, \\ L &= -\frac{1}{18} \sum_{i,j} \omega^{i} J_{ij} \,, \\ M &= -\frac{1}{18} \sum_{i,j} \omega^{j} J_{ij} \,, \\ N &= -\frac{1}{18} \sum_{i,j} \omega^{-i-j} J_{ij} \,, \end{aligned} \tag{10}$$

which are found to be

$$K=\tfrac{1}{18}(-2J_c+2J_c'-J_d+J_r)\,,$$

$$L=M=\tfrac{1}{18}(J_c-J_c'-J_d+J_r)\,,$$

$$N=\tfrac{1}{18}(J_c+2J_c'-J_d-2J_r)\,. \tag{11}$$

On the basis $\sqrt{\tfrac{1}{2}}(a+c)$, $\sqrt{\tfrac{1}{2}}(b+d)$, $\sqrt{\tfrac{1}{2}}(a-c)$, and $\sqrt{\tfrac{1}{2}}(b-d)$ the matrices are

$$\mathcal{H}_{ex}=(E_0+\tfrac{5}{4}J)I+\begin{pmatrix} -K & 5L-N & 0 & 0 \\ 5L-N & -K & 0 & 0 \\ 0 & 0 & K & 5L+N \\ 0 & 0 & 5L+N & K \end{pmatrix} \tag{12}$$

if $S=1$, and

$$\mathcal{H}_{ex}=(E-\tfrac{3}{4}J)I+\begin{pmatrix} 3K & -3L+3N & 0 & 0 \\ -3L+3N & 3K & 0 & 0 \\ 0 & 0 & -3K & -3L-3N \\ 0 & 0 & -3L-3N & -3K \end{pmatrix} \tag{13}$$

if $S=2$. I is the unit matrix and E_0 denotes the energy difference $^2E-{}^4A_2$. Diagonalization of the matrices (12) and (13) yields the eigenvalues and eigenvectors given in Table I.

It is useful to determine the transformation properties of the pair states in the local C_{2v} symmetry. Using the character tables and the notation of Koster *et al.*,[31] it can be shown that each of the wave functions of the pair states transforms as an irreducible representation of the point group C_{2v} and the results for the (^2E, $^4A_2$) states are given in Table I. The ($^4A_2$, $^4A_2$) wave functions belonging to the $S=0$ and $S=2$ levels transform as Γ_2, those belonging to the $S=1$ and $S=3$ levels transform as Γ_1 of C_{2v}.

From Table I it can be seen that we have eight energy levels which are fixed by four constants J, N, K, and L. In order to determine these four constants we must find at least four levels of the excited state. The orbital exchange parameters J_c, J_c', J_d, and J_r are in terms of J, K, L, and N:

$$\begin{aligned} J_c &= -4K+4L+J+2N\,, \\ J_c' &= 2K-2L+J+2N\,, \\ J_d &= -4K-8L+J-4N\,, \\ J_r &= 2K+4L+J-4N\,. \end{aligned} \tag{14}$$

Now let us consider the influence of spin-orbit coupling and trigonal field on the energy levels of the nn pairs. The combined action of H_{so} and V_{trig} is responsible for the 40-cm^{-1} splitting of the ^2E state of the single Cr^{3+} ions (see Sec. IV). It can be shown that this perturbation has only nondiagonal elements on the basis formed by the eigenfunctions (represented by their Γ and S value) of the ($^4A_2$, ^2E) levels as given in Table I. Therefore, no first-order spin-orbit splitting of the levels occurs. The off-diagonal elements, coupling the different excited-state levels, are found to be at most $\lambda/\sqrt{6}$, with $\lambda=40$ cm^{-1}. The energy differences between the levels is of the order of 100 cm^{-1}, and so the second-order splittings may be about 2 cm^{-1}. However, anticipating the results of Secs. IV and V, we have found that two levels (interpreted as $^5\Gamma_3$ and $^3\Gamma_1$) have a distance of 26 cm^{-1} only. The spin-orbit interaction between these two levels has matrix elements $\lambda(4-m_s^2)^{1/2}/4\sqrt{3}$, where m_s is the quantum number of total spin S, leading to a splitting of about 6 cm^{-1}. The linewidths are about 10 cm^{-1}, and so the spin-orbit splittings of the levels are not resolved, which indeed has been found experimentally. This justifies the neglect of the spin-orbit coupling and trigonal field throughout this paper.

TABLE I. Energies, wave functions, and irreducible representations (I.R.) of the ($^4A_2$, ^2E) pair states.

Total spin	Energy	Wave function[a]	I.R. of C_{2v}
$S=1$	$E_0+\frac{5}{4}J-K+5L-N$	$\frac{1}{2}(a+b+c+d)$	Γ_1
	$E_0+\frac{5}{4}J-K-5L+N$	$\frac{1}{2}(a-b+c-d)$	Γ_3
	$E_0+\frac{5}{4}J+K+5L+N$	$\frac{1}{2}(a+b-c-d)$	Γ_2
	$E_0+\frac{5}{4}J+K-5L-N$	$\frac{1}{2}(a-b-c+d)$	Γ_4
$S=2$	$E_0-\frac{3}{4}J+3K-3L+3N$	$\frac{1}{2}(a+b+c+d)$	Γ_1
	$E_0-\frac{3}{4}J+3K+3L-3N$	$\frac{1}{2}(a-b+c-d)$	Γ_3
	$E_0-\frac{3}{4}J-3K-3L-3N$	$\frac{1}{2}(a+b-c-d)$	Γ_2
	$E_0-\frac{3}{4}J-3K+3L+3N$	$\frac{1}{2}(a-b-c+d)$	Γ_4

[a]We give the abbreviations; full expressions can be found in the text.

C. Selection Rules

In a normal spinel Cr^{3+} ions occupy octahedral (B) sites, which have inversion symmetry. Therefore, both the single-ion R lines as well as many of the $({}^4A_2, {}^4A_2) \rightarrow ({}^2E, {}^4A_2)$ pair lines may be expected to be magnetic dipole (m.d.) transitions. The single-ion ${}^4A_2 \rightarrow {}^2E$ m.d. transition is only allowed through the action of the spin-orbit coupling which mixes the ${}^2E$ with the ${}^4T_2$ state.[32,37] It can then be shown that for the Cr^{3+} pairs the selection rules for m.d. transitions are

$$\Delta S = 0, \pm 1\,, \quad \Delta m_S = 0, \pm 1\,, \tag{15}$$

where S is the total spin of the pair.

For the Cr^{3+} pairs there is a mechanism which makes electric dipole transitions allowed—the exchange-induced dipole moment (e.i.d.), first proposed by Tanabe *et al.*[33] to explain magnon and magnon sideband intensities in MnF_2 and FeF_2. In the Appendix quantum-mechanical expressions for the e.i.d. are given.

It can be shown that if the electrons stay within the same orbitals (as is the case for the ${}^4A_2 \rightarrow {}^2E$ transition of Cr^{3+}), then the operator equivalent of the e.i.d. may be expressed as follows[33]:

$$\vec{\mathcal{P}}_{ex} = \sum_{i,j} \vec{P}_{ij} \vec{s}_{iA} \cdot \vec{s}_{jB}\,, \tag{16}$$

where i, j run over the three t_{2g} orbitals.

First we note that $\vec{\mathcal{P}}_{ex}$ commutes with the total spin S; this means that the selection rules for the matrix elements of the e.i.d. are

$$\Delta S = 0\,, \quad \Delta m_S = 0\,. \tag{17}$$

Application of the symmetry elements C_2^z, σ_v, and σ_v' of the point group C_{2v} of a n.n. pair leads to the following relations among the $\vec{P}_{ij}$:

$$\begin{aligned} &P^z_{ij} = P^z_{ji}\,, && P^z_{\xi\xi} = P^z_{\eta\eta}\,, \\ &P^z_{\eta\zeta} = P^z_{\xi\zeta}\,, && P^{x,y}_{ij} = -P^{x,y}_{ji}\,, \\ &P^x_{\xi\eta} = -P^y_{\eta\xi}\,, && P^x_{\eta\zeta} = -P^y_{\xi\zeta}\,, \\ &P^x_{\xi\xi} = -P^y_{\xi\eta}\,, \end{aligned} \tag{18}$$

where $i, j = \xi, \eta, \zeta$ and x, y, z denote the components in a coordinate frame, centered in M and parallel to the x, y, z axes centered on the Cr^{3+} ions (Fig. 1).

It follows from (18) that $P^{x,y}_{ii} = 0$ for all i and we are left with 3 constants,

$$P_1 = P^x_{\xi\eta}\,, \quad P_2 = P^x_{\xi\xi}\,, \quad P_3 = P^x_{\eta\zeta} \tag{19}$$

from which the P^x and P^y matrices can be built:

$$P^x = \begin{pmatrix} 0 & P_1 & P_2 \\ -P_1 & 0 & P_3 \\ -P_2 & -P_3 & 0 \end{pmatrix}\,,$$

$$P^y = \begin{pmatrix} 0 & P_1 & -P_3 \\ -P_1 & 0 & -P_2 \\ P_3 & P_2 & 0 \end{pmatrix}\,. \tag{20}$$

The P^z matrix becomes

$$P^z = \begin{pmatrix} P^z_{\xi\xi} & P^z_{\xi\eta} & P^z_{\xi\zeta} \\ P^z_{\xi\eta} & P^z_{\xi\xi} & P^z_{\xi\zeta} \\ P^z_{\xi\zeta} & P^z_{\xi\zeta} & P^z_{\zeta\zeta} \end{pmatrix}\,, \tag{21}$$

where we have four different constants $P^z_{\xi\xi}$, $P^z_{\zeta\zeta}$, $P^z_{\xi\eta}$, $P^z_{\xi\zeta}$.

The matrix elements of the e.i.d. between the ground-state and excited-state spin multiplets can be calculated using the matrix elements given by Pryce[26]:

$$\left.\begin{aligned} \langle AA|P^{x,y,z}|a\rangle &= -\sqrt{18}\,L_{x,y,z} \\ \langle AA|P^{x,y,z}|b\rangle &= -\sqrt{18}\,L^*_{x,y,z} \\ \langle AA|P^{x,y,z}|c\rangle &= +\sqrt{18}\,M_{x,y,z} \\ \langle AA|P^{x,y,z}|d\rangle &= +\sqrt{18}\,M^*_{x,y,z} \end{aligned}\right\} \text{ for } S=2\,,$$

$$\left.\begin{aligned} \langle AA|P^{x,y,z}|a\rangle &= -\sqrt{10}\,L_{x,y,z} \\ \langle AA|P^{x,y,z}|b\rangle &= -\sqrt{10}\,L^*_{x,y,z} \\ \langle AA|P^{x,y,z}|c\rangle &= -\sqrt{10}\,M_{x,y,z} \\ \langle AA|P^{x,y,z}|d\rangle &= -\sqrt{10}\,M^*_{x,y,z} \end{aligned}\right\} \text{ for } S=1\,, \tag{22}$$

where, for x polarization,

$$L_x = \frac{1}{18}\sum_{i,j} \omega^i P^x_{ij} = \tfrac{1}{18}\left[i\sqrt{3}\,P_1 + (-\tfrac{3}{2} + \tfrac{1}{2}i\sqrt{3})P_2 + (-\tfrac{3}{2} - \tfrac{1}{2}i\sqrt{3})P_3\right]\,, \tag{23a}$$

$$M_x = \frac{1}{18}\sum_{i,j} \omega^j P^x_{ji} = -L_x\,,$$

and for y polarization,

$$L_y = -M_y = \tfrac{1}{18}\left[i\sqrt{3}\,P_1 + (\tfrac{3}{2} + \tfrac{1}{2}i\sqrt{3})P_2 + (\tfrac{3}{2} - \tfrac{1}{2}i\sqrt{3})P_3\right]\,. \tag{23b}$$

We define

$$P_4 = -P^z_{\xi\xi} + P^z_{\zeta\zeta} + P^z_{\xi\zeta} - P^z_{\xi\eta}\,; \tag{24}$$

then we find for z polarization

$$L_z = M_z = \tfrac{1}{18}P_4\,. \tag{25}$$

It can easily be shown that P^z transforms as Γ_1 of C_{2v}, but P^x and P^y do not transform as an irreducible representation of C_{2v}. Therefore, we take the combinations $P^X = (1/\sqrt{2})(P^x - P^y)$ and $P^Y = (1/\sqrt{2})(P^x + P^y)$; P^X transforms as Γ_2, P^Y as Γ_4 of C_{2v}. The results are given in Table II, where the ground-state levels and excited-state levels are designated by ${}^{(2S+1)}\Gamma_\nu$, where S is the total spin, and Γ_ν is the irreducible representation

TABLE II. Matrix elements of the exchange-induced electric dipole moment between ground-state and excited-state levels. $P^X = (1/\sqrt{2})(P^x - P^y)$ transforms on Γ_2, $P^Y = (1/\sqrt{2})(P^x + P^y)$ as Γ_4 and $P^Z = P^z$ as Γ_1 of C_{2v}.

Ground-state level	Excited-state level	$\langle AA \mid P^X \mid AE\rangle$	$\langle AA \mid P^Y \mid AE\rangle$	$\langle AA \mid P^Z \mid AE\rangle$
$AA^3\Gamma_1$	$AE^3\Gamma_4$	0	$-i\sqrt{\frac{5}{27}}(2P_1 + P_2 - P_3)$	0
$AA^3\Gamma_1$	$AE^3\Gamma_1$	0	0	$-\frac{1}{9}\sqrt{10}\,P_4$
$AA^3\Gamma_1$	$AE^3\Gamma_2$	$\frac{1}{3}\sqrt{5}\,(P_2 + P_3)$	0	0
$AA^3\Gamma_1$	$AE^3\Gamma_3$	0	0	0
$AA^5\Gamma_2$	$AE^5\Gamma_2$	0	0	$-\frac{1}{9}\sqrt{18}\,P_4$
$AA^5\Gamma_2$	$AE^5\Gamma_3$	0	$-i\sqrt{\frac{1}{3}}(2P_1 + P_2 - P_3)$	0
$AA^5\Gamma_2$	$AE^5\Gamma_4$	0	0	0
$AA^5\Gamma_2$	$AE^5\Gamma_1$	$P_2 + P_3$	0	0

of C_{2v} of the level, according to Table I. The transition probabilities are, of course, given by the square of the matrix elements.

IV. EXPERIMENTS

A. Optical Spectra of Single Cr^{3+} Ions

In this section we describe the luminescence and absorption spectra of single Cr^{3+} ions in $ZnGa_2O_4$, especially to determine the nature of the pure electronic and phonon assisted transitions (electric or magnetic dipole transitions) and to gain knowledge of the vibronic sideband frequencies. These matters are important for the interpretation of the pair spectra.

Recently Kahan and Macfarlane[34] have reported the emission spectrum of $ZnGa_2O_4$: Cr, but no detailed interpretation of the lines was given and no attention has been paid to the vibronic sidebands.

An emission spectrum of a single crystal $ZnGa_{1.999}Cr_{0.001}O_4$ at 77 °K is shown in Fig. 3. The R lines are situated at 6854.2 and 6873.0 Å, their separation being 40 cm^{-1}. The width at half-height

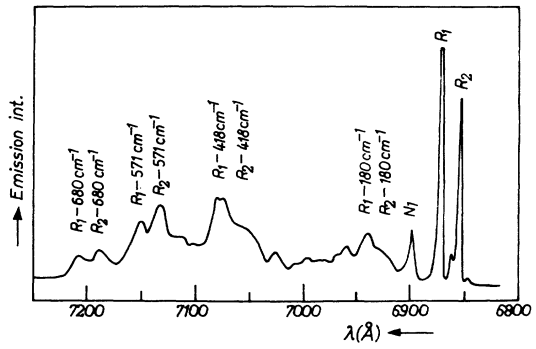

FIG. 3. Luminescence spectrum of a single crystal $ZnGa_{1.999}Cr_{0.001}O_4$ at 77 °K. The strongest vibronics are indicated. Excitation at 5145 Å (the same spectra are obtained with excitation at 5600, 4300, or 2537 Å).

of the lines amounts to 5 cm^{-1}. At the long-wavelength side of the R lines the vibronic sidebands are clearly visible. By comparing the spectra at 300, 77, and 4.2 °K we determined the vibronic sideband frequencies as follows:

(i) At 77 and 300 °K the vibronic peaks should occur in "pairs" with separation 40 cm^{-1}.

(ii) The vibronic peaks corresponding to R_2 (and R_2 itself) must be absent at 4.2 °K.

(iii) At room temperature the anti-Stokes lines of the vibronics must be present.

The peaks in the spectra which fulfill these three demands are regarded as certainly identified vibronic sidebands of the R lines. The frequencies and intensities (qualitatively) of these vibronics are given in Table III.

The remaining lines in the spectrum (Fig. 3) can be divided into three groups:

(i) The line at 6899 Å (designated by N_1) and its vibronics; as we shall see later this line is possibly a pair line and will be described in Sec. IV B.

(ii) Two lines close to the R lines at 6848 and 6862 Å from which the 6848-Å line disappears at low temperatures. The intensities of these lines were found to be independent of the chromium con-

TABLE III. Vibronic sideband frequencies of $ZnGa_2O_4$: Cr^{3+} and phonon frequencies of $ZnGa_2O_4$.

Vibronic sideband frequency (± 5 cm^{-1}) (in cm^{-1})	Intensity	$k = 0$ phonon frequency; pure $ZnGa_2O_4$ from infrared and Raman spectroscopy Ref. 36	Ref. 35	Character
140	weak	175	175	T_{1u}
180	medium	328	333	T_{1u}
258	weak	420	455	T_{1u}
325	weak	570	593	T_{1u}
418[a]	strong	467		T_{2g}
532	weak	611		T_{2g}
571	strong	674		E_g
680	medium	714		A_{1g}

[a]A doublet with separation of the components 6 Å.

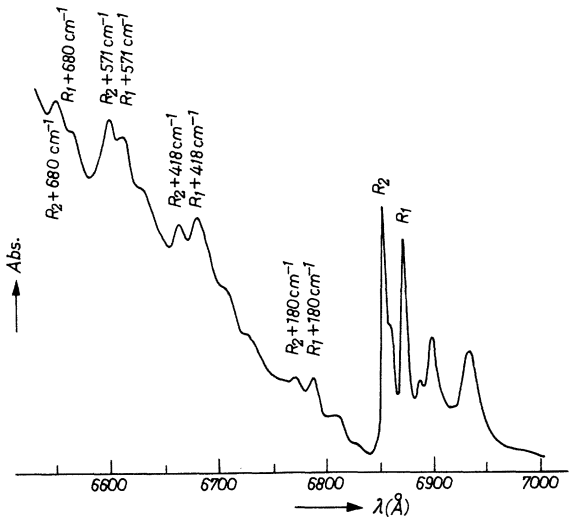

FIG. 4. Absorption spectrum of a single crystal $ZnGa_{2-x}Cr_xO_4$ with $x \approx 0.035$ at $T = 10\,^\circ K$.

centration, but in the crystals these lines were stronger than in the powder samples. Possibly these lines are the R lines of another Cr^{3+} center (with different ^2E-$^4A_2$ separation and different ^2E splitting) which occurs in greater concentration in the crystals than in the powders.

(iii) Some very weak lines which are much like ordinary vibronics but which do not fulfill all demands as given above. We shall disregard these lines further because they are of no importance to us.

Absorption spectra could only be measured on heavily doped crystals (because of the low oscillator strength) which were of rather poor optical quality; the R linewidth in absorption was about 8 cm^{-1}. An absorption spectrum recorded at 10 °K is shown in Fig. 4. The vibronics of the R lines are now, of course, at the blue side of the R lines; the lines at the red side together with the line at 6830 Å (weakly visible) will be discussed in Sec. IV B. The vibronic sideband frequencies have been determined and were found to be identical (within the experimental errors) with those found in the emission spectra; the relative intensities of the vibronic peaks were the same in both cases.

The vibronic sideband frequencies of the Cr^{3+} R lines may correspond to phonon frequencies of the pure $ZnGa_2O_4$ lattice or to local mode frequencies. Local modes can occur because of the mass difference between Cr and Ga. Recently, infrared[35,36] and Raman[36] measurements have been reported; the results of Refs. 35 and 36 are given in Table III. The four infrared-active modes have T_{1u} character, the Raman-active modes are all of even parity: three T_{2g}, one E_g, and one A_{1g}.[36] One observes that the vibronic sidebands at 180, 325, 418, and 571 cm^{-1} are very close in frequency to the four T_{1u} ($k = 0$) phonon frequencies of the pure lattice. It is therefore very likely that these four vibronic sidebands of the $^2E \rightarrow {}^4A_2$ transition are due to coupling to these T_{1u} vibrations.

Now let us consider the oscillator strengths of the electronic (R line) transitions. Since the Cr^{3+} ion is at a site with inversion symmetry the zero phonon lines should be magnetic dipole transitions. In MgO: Cr^{3+} it has indeed been found[37,38] that the R line is a magnetic dipole and the vibronic sidebands are electric dipole transitions. The oscillator strength for a magnetic dipole transition is given by

$$f = (1/nN_0)\,(mc/\pi e^2) \int \alpha(\nu)\, d\nu\,, \tag{26}$$

where n is the refractive index (= 1.74 for $ZnGa_2O_4$), N_0 is the number of Cr^{3+} ions per cm^3, and the other symbols have their usual meaning;

$$\alpha(\nu) = (1/d_0)\ln(I_0/I) \tag{27}$$

is the absorption coefficient (cm^{-1}), where d_0 is the thickness of the crystal. The difficulty in deciding what has to be included in $\int \alpha(\nu)\, d\nu$ has been resolved in the same way as in Ref. 14. For a crystal containing about 7.10^{19} Cr^{3+}/cm^3 ($x = 0.03$–0.04, inhomogeneous) we find at $T = 77$ °K, 4.2% absorption for a crystal of 4-mm thickness with an R linewidth of 8 cm^{-1}. This leads to $f = 6.10^{-9}$ for both R lines, with an uncertainty of about 30%. Kahan and Macfarlane[34] calculate the m.d. oscillator strength for R_1 and R_2 as 5.4×10^{-9}, which is close to the experimental value. Therefore, we conclude that the R lines are m.d. transitions.

The luminescence decay time is connected with the oscillator strength f through

$$f\tau = \frac{mc^3}{8\pi^2 e^2 \nu^2}\,\frac{1}{n^3} = 1.5\times10^{-9}\ \text{sec}.$$

With $f = 6\times10^{-9}$ we find $\tau_{calc} = 250$ msec. About 18% of the luminescence occurs in the R lines, which leads to $\tau_{calc} = 45$ msec when corrected for sideband intensity. The measured value is $\tau_{obs} = 14$ msec. This indicates a quantum efficiency of about 30% which is a reasonable value, also found in other spinels.[14]

B. Spectra of Exchange-Coupled Cr^{3+} Pairs

1. Luminescence Spectra

In this subsection we investigate more heavily Cr^{3+}-doped $ZnGa_2O_4$. First we examine the emission spectra. By looking at the concentration dependence and optical decay times of the extra lines appearing at high Cr^{3+} concentrations we shall determine which lines are due to specific pairs of Cr^{3+} ions.

The emission spectrum of $ZnGa_{2-x}Cr_xO_4$ powder

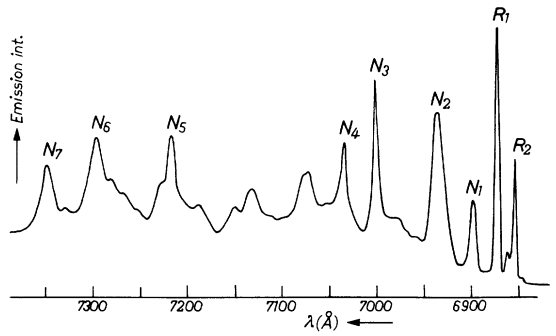

FIG. 5. Luminescence spectrum of $ZnGa_{2-x}Cr_xO_4$ powder with $x=0.016$ at $T=77$ °K. Excitation at 5145 Å. This spectrum has been recorded using a time-resolved spectroscopy technique (exciting light chopped) which enhances the pair lines relative to the single-ion lines, owing to the shorter decay time of the pairs.

with $x=0.016$ is shown in Fig. 5. Comparing it with Fig. 3 we observe the following:

(i) The line at 6899 Å (N_1) has increased relative to the R lines.

(ii) A new strong broad line (half-width 30 cm^{-1}) has appeared at 6935 Å (N_2).

(iii) A new strong, relatively sharp line (half-width 10 cm^{-1}) at 7003 Å (N_3) and a doublet (N_4) at 7034 Å and 7039 Å have shown up.

(iv) The rather broad lines at 7218 Å (N_5), 7297 Å (N_6), and 7350 Å (N_7) and the smaller peaks in the neighborhood are all new.

So we expect that at least some of these lines are due to Cr^{3+} ion pairs. By measuring emission spectra from a series of powders [the Cr^{3+} concentration in these powders was well known (Sec. II)] we determined the concentration dependence of these lines relative to R_1 and the result is given in Fig. 6. Since, assuming a statistical distribution of the Cr^{3+} over the Ga sites, the number of pairs increases with the square and the single ions with the first power of the concentration, we expect the ratio of the emission intensities of a pair line to an R line to increase linearly with the chromium concentration. From Fig. 6 it can be seen that none of the lines N_1–N_7 shows this linear concentration dependence. In fact N_3–N_7 all behave in the same way (N_5–N_7 are not shown in Fig. 6) and vary at not too high concentrations as x^3, N_2 as $x^{0.6}$, and N_1 as $x^{0.3}$, all relative to R_1. We believe that this is caused by energy transfer effects.[39] It is apparent that $N_3 - N_7$ belong to the same center because of their similar behavior. Looking at the energy differences we observe that N_5–N_7 are situated at approximately 420, 570, and 680 cm^{-1} from N_3, respectively, and so we interpret N_5–N_7 as vibronics of N_3 (see Table III). Since the distance $N_3 - N_4$ is 63 cm^{-1} and this does not correspond to a phonon frequency, we conclude that N_4 is not a vibronic of N_3. It is remarkable (Fig. 5) that N_5–N_7 are very strong relative to N_3: roughly a factor of 10 stronger (integrated emission intensity). This ratio differs much from the ratio of the 420, 570, and 680 cm^{-1} vibronics of R_1 relative to R_1 (see, for instance, Fig. 3), which is about 2. This phenomenon will be discussed later.

Luminescence decay times have been measured for all the lines in the emission spectrum. The measurements were performed at 77 °K on powders with different Cr^{3+} concentrations. The results are given in Fig. 7, where the decay times (τ) of R_1, N_1–N_3 are given; R_2 and the vibronics of R_1 and R_2 were found to have the same τ as R_1; N_4–N_7 were the same as N_3. The concentration dependence of the decay times is most probably caused by energy transfer effects, for instance the abrupt decrease of the decay time of R_1 above $x \approx 0.006$ is, according to Lyo,[40] connected with a delocalization of the single-ion excitation. At any concentration we find $\tau_{R_1} > \tau_{N_1} > \tau_{N_2} > \tau_{N_3}$. Owing to the existence of the exchange-induced dipole moment, it is to be expected that n.n. pairs have a shorter decay time than second-neighbor pairs, and so on. On these grounds we assign N_3 and N_4 (and of course N_5–N_7) to transitions within the nearest-neighbor-pair system, N_2 to second-neighbor pairs and N_1 to third-neighbor pairs. However, these last two assignments are uncertain because we expect the lines due to second and third neighbors to lie close to the R lines because the exchange parameters for these pairs are of the order of a few cm^{-1},[17] while the red shift of N_1 and N_2 relative to R_1 is 55 and 131 cm^{-1}, respectively. The interpretation that N_3 and N_4 are n.n. lines is to some extent supported by the concentration dependence of the lines if we assume that energy transfer takes place most efficiently from the single ions to the nn pairs,

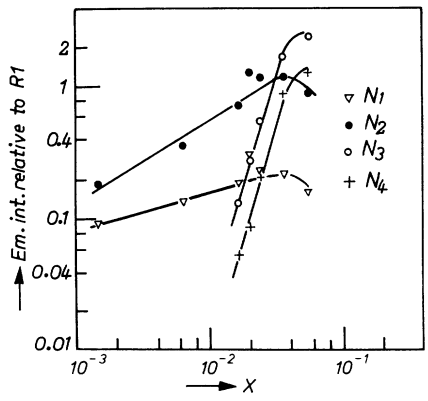

FIG. 6. Emission intensity (peak value) of N_1–N_4 relative to the intensity of R_1 as a function of concentration at $T=77$ °K. N_5–N_7 are not shown in the figure, for reasons of clarity, but behave in the same way as N_3 and N_4.

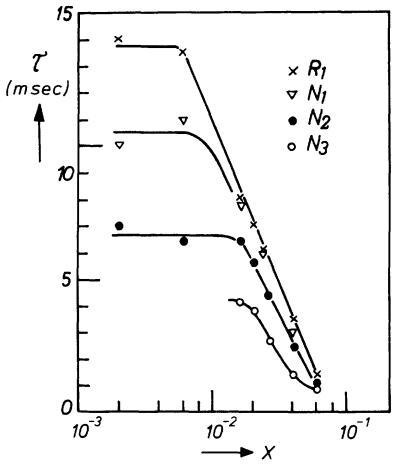

FIG. 7. Luminescence decay times of powders $ZnGa_{2-x}Cr_xO_4$ as a function of x at $T=77$ °K. The lines N_3 and N_4 are superimposed on strong R line vibronics. Therefore, the measured decay times of N_3 and N_4 are too long because the decay time of these vibronics is longer than that of N_3 and N_4. This effect is concentration dependent because the intensity ratio N_3 (and N_4) to the R line vibronics varies with the Cr^{3+} concentration. In order to find the true decay times of N_3 and N_4, we have used a time-resolved spectroscopy technique, which enabled us to separate the lines N_3 and N_4 from the vibronics. The result is, for $x=0.016$, $\tau_{N_3}=\tau_{N_4}=(1.8\pm0.3)$ msec.

which in fact is to be expected at 77 °K.[39]

The emission spectrum of a heavily doped sample has been measured in the temperature range (4.5–180)°K. The relative intensities of some of the lines varied with temperature (probably mainly due to energy transfer processes) but no extra lines were found and the intensity ratio of N_3 to N_4 remained unchanged. This means for the n.n. pair system that (i) N_3 and N_4 belong to the same excited-state level which is the lowest in energy, and (ii) no other levels within, say, 100 cm^{-1} above this lowest level are present.

We conclude that the emission measurements yield too little information to allow deduction of either the ground-state or excited-state exchange splittings. In other comparable cases[27,41–44] ground-state exchange splittings could be found from the luminescence spectrum; the main reason for the failure in this case is the strong vibronics of the R lines, which mask the expected pair transitions from the lowest excited state to the other two spin multiplets of the ground state.

One puzzling fact is the doublet character of N_4, the separation of the components amounts to 11 cm^{-1}. Since splittings of the spin multiplets of the ground state are at most a few cm^{-1} (the trigonal zero-field-splitting parameter[20,34] $D=0.523$ cm^{-1}), one would expect that this is due to a splitting of the excited-state level [e.g., due to spin-orbit coupling and trigonal field (Sec. III B)]. In that case pronounced thermalization effects should occur between the two components in the emission spectrum in the temperature range (5–20) °K. Such effects are, however, not observed. In fact the intensity ratio of both components is independent of the temperature (Fig. 8). Another observation concerning this problem is the following. We have measured an emission spectrum of a powder with $x=0.04$; the two components are found at 7034 Å and 7039 Å, with the 7034 Å component about twice as large as the other. A single crystal with about the same x exhibits broader lines than the powder and the component at 7039 Å is now about as strong as the 7034 Å one. This could mean that the 7039 Å component is due to a slightly different Cr^{3+} pair which occurs in larger concentrations in the crystals than in the powder. Apparently, the corresponding splitting of N_3 is smaller and not resolved.

2. *Absorption Measurements*

Part of an absorption spectrum of a heavily doped ($x=0.03$–0.04, inhomogeneous) crystal, at two temperatures is given in Fig. 9. Not shown are the vibronics at the blue side of the R lines. In Fig. 9, apart from the R lines one clearly recognizes lines N_1 and N_2 which are found to be nearly independent of temperature; N_3 and N_4 are not present at low temperatures but appear at elevated temperatures. Two new lines are visible which are not present in the luminescence spectra, which we shall call N_8 at 6887.8 Å and N_9 at 6829.6 Å. It was found that the intensity of R_2 was larger than R_1 and the difference R_2-R_1 was temperature dependent, due to a variation of the intensity of R_2 (R_1 was nearly independent of temperature). Since R_2 by itself is expected to be temperature independent, this means that there is another line coinciding with R_2 which decreases with in-

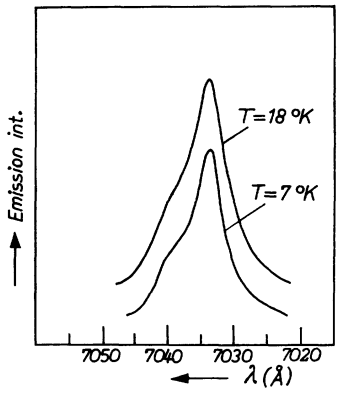

FIG. 8. Emission line N_4 observed at $T=7$ and 18 °K; instrumental resolution 1 Å.

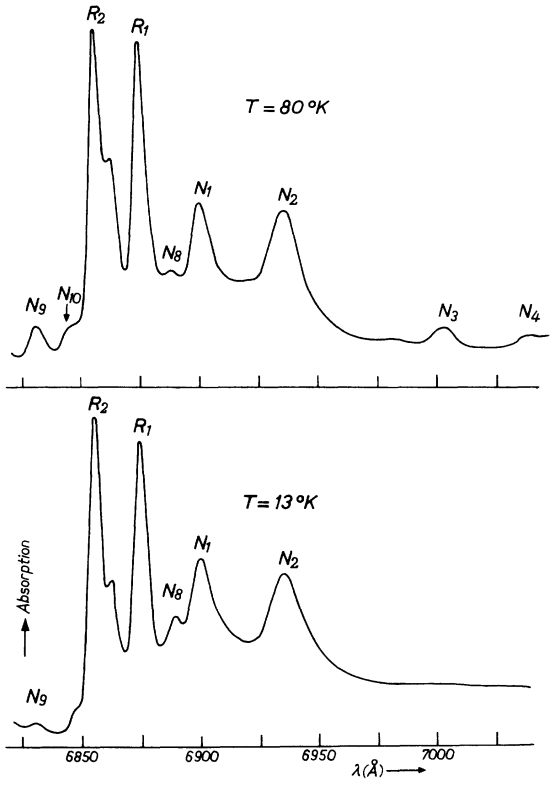

FIG. 9. Absorption spectrum at $T=13$ and 80 °K (the sample is the same as that used for Fig. 4).

creasing temperature. Owing to a serious baseline problem the precise determination of $R_2 - R_1$ is rather difficult.

The intensities of the lines N_3, N_4, N_8, N_9 and the difference $R_2 - R_1$ as a function of temperature are given in Fig. 10. Since the lines are very weak, we have measured the spectra several times and the values given in Fig. 10 are averages over these measurements; yet the measuring inaccuracy, also indicated in Fig. 10, is rather large. The absorption intensity of a line is proportional to the occupation number $n(S)$ of the level with spin S from which the transition starts. $n(S)$ is given by

$$n(S) = [(2S+1)/Z_a]\, e^{-E(S)/kT}\,, \tag{28}$$

where Z_a is the partition function

$$Z_a = \sum_{S=0}^{3} (2S+1)\, e^{-E(S)/kT}\,. \tag{29}$$

The $E(S)$ are given by expression (2).

It can be seen that the temperature dependence of N_3, N_4, N_8, and N_9 (Fig. 10) can be fitted reasonably well using the exchange Hamiltonian (1) with

$$J = -22 \pm 2 \text{ cm}^{-1}\,, \quad j = -2 \pm 1 \text{ cm}^{-1}\,.$$

It follows that the transition N_3 starts on the ground-state $S=2$ level, N_4 on $S=3$, N_8 on $S=0$, and N_9 on the $S=1$ level.

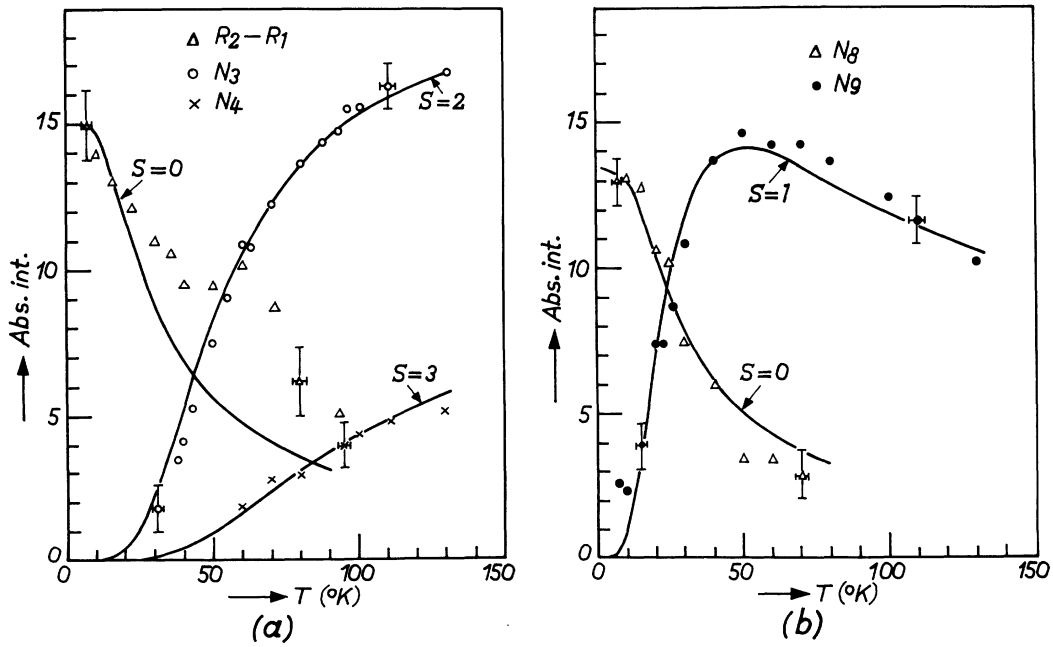

FIG. 10. Absorption intensity of N_3, N_4, N_8, N_9, and R_2-R_1 as a function of temperature. The values given are peak intensities, but the linewidths are constant in the range (4–120)°K and therefore the peak values are proportional to the integrated absorption intensities. The intensity units are arbitrary and may be different for each line. The drawn curves ($S=0,1,2,3$) are calculated from Eqs. (28) and (29) with $J=-22$ cm^{-1} and $j=-1.7$ cm^{-1}, multiplied by a constant to obtain the best fit to the experimental points.

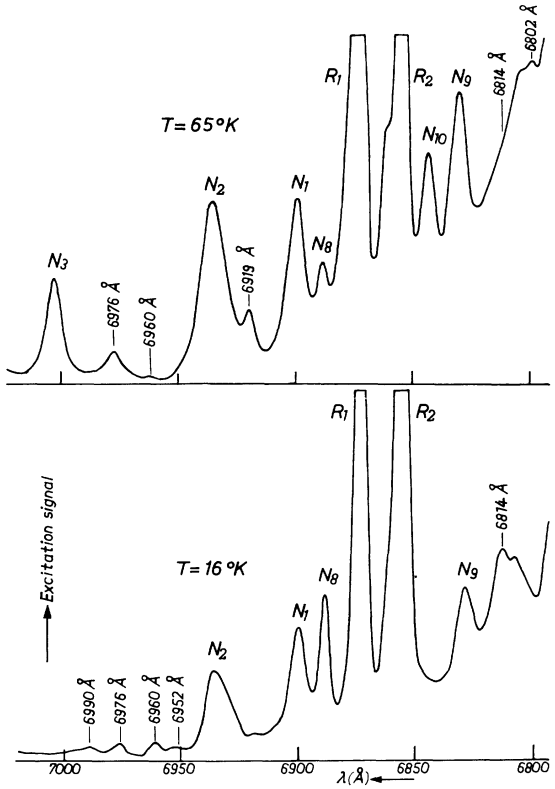

FIG. 11. Luminescence excitation spectrum of $ZnGa_{2-x}Cr_xO_4$ powder with $x=0.036$ at $T=16$ and 65 °K. The luminescence in the range 7250–7400 Å is monitored while irradiating the sample with monochromatic light with wavelength λ.

We have found that a shoulder at 6843 Å appears at higher temperatures (N_{10}). Qualitatively this shoulder behaves as an $S=2$ line, but due to the very poor resolution of the line we cannot be certain about this. From Fig. 10 it can be seen that N_9 deviates from the theoretical curve at low temperatures. Apparently N_9 coincides with another line which remains at low temperatures. Further we see that the difference R_2-R_1 behaves qualitatively as an $S=0$ line but quantitatively it deviates from the theoretical $S=0$ curve. This might be caused by the base-line problem but it is also possible that the line coinciding with R_2 does not belong to the n.n. pairs.

In conclusion we remark that we have established the ground-state exchange parameter J and j and three levels in the excited state with certainty, using the fact that we now know on which levels N_3, N_4, N_8, and N_9 start (N_3 and N_4 terminate on the same excited-state level).

3. *Excitation Measurements*

In this subsection we describe the luminescence excitation spectra of nn pair lines. In these measurements the intensity of the pair line which is situated at the longest wavelength is monitored while the sample is irradiated with monochromatic light of varying wavelength. In fact we have used the vibronics of N_3 for this purpose; this means that only fluorescence light in the range 7250–7400 Å was selected by a $\frac{1}{4}$-m Jarrel-Ash monochromator.

It is clear that the excitation signal is proportional to the absorption but excitation measurements have certain advantages over absorption measurements:

(i) The signal-to-noise ratio is better, mostly for experimental reasons: in absorption one has a large light signal on which very small variations are to be measured, while in the excitation measurement no light is incident on the photomultiplier when there is no absorption and shot noise and small disturbances in the optical path are much less important.

(ii) In the absorption measurement one needs a large single crystal; in the excitation experiment there is no need for this, in fact powders can be used. This has several advantages, e.g., the powders exhibited narrower lines than the crystals.

(iii) The intensities of the n.n. pair lines are enhanced relative to the lines of other centers (e.g., single Cr^{3+} ions), which are observed via energy transfer effects.

In Fig. 11 excitation spectra of a powder sample with $x=0.036$ at two temperatures are shown. Besides the lines which were already found in absorption, a number of other lines are now visible. The temperature dependence of all the important lines has been measured, and the result is given in Fig. 12. As stated before, the R lines are found because of energy transfer from the single ions to the n.n. pairs and the temperature dependence of R_1 is apparently due to the temperature dependence of the transfer process (see Fig. 12). The intensities of the lines N_1 and N_2 (not shown in Fig. 12) show a dependence similar to that of R_1.

The temperature dependences of the lines N_3, N_8, and N_9 can be fitted reasonably well to the theoretical curves as given by (28) and (29), although there is a deviation at high temperatures which is probably caused by energy transfer back from the n.n. pairs to the single ions. N_9 also deviates at low temperatures, as in the absorption measurements (Fig. 10).

The difference in intensities between R_2 and R_1 is seen to fall off more rapidly than the theoretical $S=0$ curve (Fig. 12), contrary to what was found in the absorption measurements. This may be caused by the fact in absorption there was a serious base-line problem while in excitation energy transfer effects occur. Therefore, we are still not sure whether the line coinciding with R_2 is an

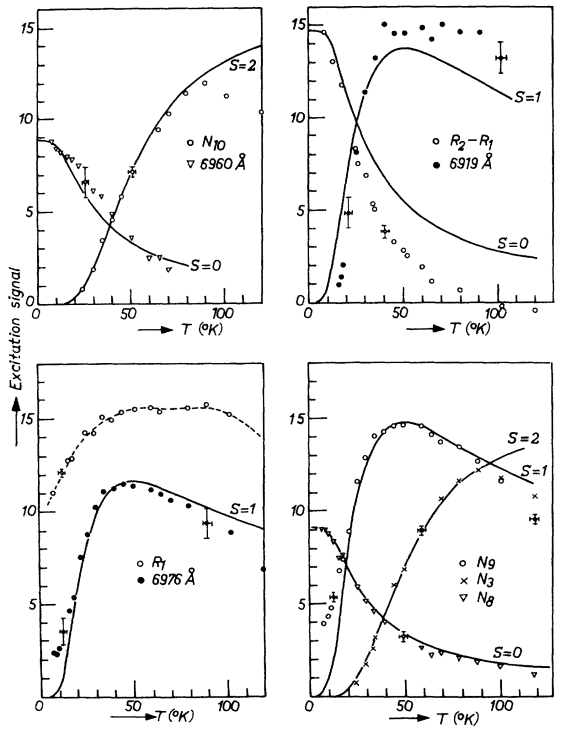

FIG. 12. Temperature dependence of the excitation line strengths for a number of lines of $ZnGa_{2-x}Cr_xO_4$ with $x=0.036$. The units are arbitrary and may be different for each line (as is reflected in the length of the bars representing the measuring inaccuracy). The drawn curves are calculated from Eqs. (28) and (29) with $J=-22$ cm^{-1} and $j=-1.7$ cm^{-1}, multiplied by a constant to obtain the best fit to the experimental points. The broken curve is a curve through the experimental points of R_1.

$S=0$ n.n. pair line or not.

Owing to the better signal-to-noise ratio and the narrower lines as compared with the absorption spectra, we are now able to observe a number of lines which were not found (or not definitely assigned) in the absorption experiments:

(i) Two $S=0$ lines: (a) A weak line at 6960 Å; its temperature dependence is given in Fig. 12 which shows that the transition starts on the $S=0$ ground-state level. (b) A line at 6814 Å, which is poorly resolved from vibronics of the R lines. Owing to this poor resolution, we cannot measure its intensity accurate, qualitatively it behaves as an $S=0$ line.

(ii) Two $S=1$ lines: (a) A weak line at 6976 Å; its temperature dependence is given in Fig. 12. (b) When the line N_1 is slowly scanned under high resolution, one clearly observes a rather strong shoulder at 6904 Å (see Fig. 13) which qualitatively behaves as an $S=1$ line.

(iii) An $S=2$ line at 6843 Å (N_{10}): This line is now very well resolved (compare with Fig. 9) and it behaves clearly as an $S=2$ line (see Fig. 12).

Although this line is situated at 333 cm^{-1} from N_3, it is very unlikely that it is a vibronic of N_3, because of the fact that in the emission spectrum no vibronic of N_3 at 333 cm^{-1} is present.

(iv) The line at 6802 Å (Fig. 11) behaves qualitatively as an $S=2$ line: This line is situated at 420 cm^{-1} from N_3 and therefore we conclude that it is a vibronic of N_3.

Also newly found are three lines which cannot be assigned as n.n. pair lines because the temperature dependence of these lines cannot be fitted to the theoretical curves of the nn pairs:

(i) A very weak line at 6952 Å, which is only visible at the lowest temperatures: The intensity of this line decreases with increasing temperature much faster than, for example, the 6960-Å ($S=0$) line.

(ii) A very weak line at 6990 Å: The temperature dependence of this line is similar to the 6952-Å line.

(iii) A weak line at 6919 Å: The temperature dependence of this line is given in Fig. 12. It cannot be fitted to $S=0$, 2, or 3 curves and the fit to an $S=1$ curve is very bad: the intensity drops off too fast at low temperatures and at high temperatures the intensity is too large (the theoretical curve has been drawn in such a way that the experimental point at $T=32$ °K is situated on the theoretical curve).

C. Experimental Line Intensities and Energy-Level Diagram

The results of emission, absorption, and excitation measurements are collected in Table IV, where we have listed all the significant zero phonon lines of the spectrum. In Table IV the integrated intensities (divided by the occupation number of the ground-state level from which the line starts) of the R lines, N_1, N_2, and nn pair lines are given too. The procedure for determining this was as follows. The integrated intensities (divided by the occupation number of the level) for R_1, R_2, N_3, N_8, and N_9 are directly obtained from the absorption spectrum (for the crystal with about 7×10^{19}

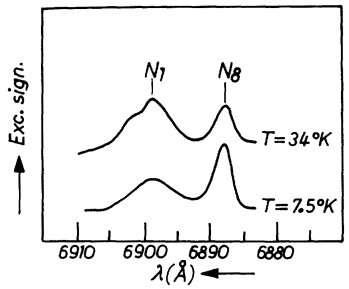

FIG. 13. Lines N_1 and N_8 in the excitation spectrum observed with instrumental resolution 1.6 Å at $T=7.5$ and 34 °K.

TABLE IV. Positions and integrated absorption intensities of all important zero-phonon lines in the spectrum.

Line designation	Observation[a] A	L	E	Line position[b] Å	cm^{-1}	Intensity[c] (arbitrary units)	Osc. strength magnetic dipole (10^{-9})	Assignment[d]	Remarks
			×	6814	14676	~15	~8	n.n. $S=0\rightarrow1$	poorly resolved
N_9	×		×	6829.6	14642	47		n.n. $S=1\rightarrow1$	
N_{10}	×		×	6843.0	14614	53		n.n. $S=2\rightarrow2$	poorly resolved in abs.
R_2	×	×	×	6854.2	14590	~135	~6	SI+n.n.?	R_2 coincides with
R_1	×	×	×	6873.0	14550	135	6	SI	other line
N_8	×		×	6887.8	14518	17	8	n.n. $S=0\rightarrow1$	
N_1	×	×	×	6898.9	14495	76[e]		3n?	
			×	6904	14485	~30		n.n. $S=1\rightarrow1$	poorly resolved
			×	6919	14453			?	
N_2	×	×	×	6935	14419	123[e]		2n?	
			×	6952	14384			?	
			×	6960	14368	2	1	n.n. $S=0\rightarrow2$	
			×	6976	14335	6	3	n.n. $S=1\rightarrow2$	
			×	6990	14306			?	
N_3	×	×	×	7003.0	14280	71		n.n. $S=2\rightarrow2$	
N_4	×	×	×	7034	14217	~40[f]	~18[f]	n.n. $S=3\rightarrow2$	
				7039	14206	~20[f]	~9[f]		

[a] A = absorption, L = luminescence, E = excitation.

[b] Accuracy in line position is ± 0.5 Å or ± 1 cm^{-1} for the sharper lines and ± 1 Å or ± 2 cm^{-1} for the broader and poorly resolved lines; T = 77 °K.

[c] Figures given here are integrated intensities divided by the occupation of the level and were determined using a sample $ZnGa_{2-x}Cr_xO_4$ with $x \approx 0.035$ (see also text).

[d] Ratio of the components sample dependent (see text).

[d] SI means single ions; n.n., 2n, 3n are nearest, second, and third neighbors, respectively.

[e] For N_1 and N_2 100% occupation of the level has been assumed.

[f] Ratio of the components sample dependent (see text).

Cr/cm^3). The intensities, divided by the occupation number of the other lines found in the excitation spectra, are then obtained by comparing their intensities with the intensities of N_3, N_8, and N_9 in the same excitation spectrum. The line N_4 could only be measured with reasonable accuracy in emission so the value given in Table IV has been determined by comparing N_4 with N_3 in an emission spectrum, and since N_4 is a doublet we give the values for both components. Some remarks:

(i) For N_9 and the 6976-Å line (both are $S=1$ lines) we have subtracted the line intensity which remains at 7 °K (Figs. 9 and 12).

(ii) We assume that no energy transfer takes place from higher excited-state levels of the n.n. pair system (transfer from the lowest level does not affect the results); this is a reasonable assumption as can be seen from the fact that the intensity ratio N_8 to N_3 is about the same in absorption and excitation.

(iii) The intensity of R_2 is uncertain because, as we have seen, another line (probably $S=0$ line of the nn pairs) coincides with R_2; at high temperatures, R_2 is about as strong as R_1 and therefore we assume identical intensities for R_2 and R_1.

(iv) Instead of the intensities, oscillator strengths could have been given in Table IV if we knew whether the lines are magnetic or electric dipole transitions. We are only certain about this for R_1 and R_2 (m.d.) and the oscillator strengths of the R lines are 6×10^{-9}. However, it seems likely that the $S=0$ lines (N_8, 6960 Å, 6814 Å), N_4, and the 6976-Å line are m.d. transitions (see also later) and for these, oscillator strengths are given too, under the assumption that the Cr^{3+} ions are statistically distributed over the Ga^{3+} sites (this means about 7×10^{19} single ions per cm^3 and about 7×10^{18} n.n. pairs per cm^3).

(v) The accuracy of the intensity figures in Table IV is not high, especially for the poorly resolved lines in the spectrum, and may range from 20 to 50%.

We will now consider the energy-level diagram of the nearest-neighbor pair system. The knowledge of the energies of the optical transitions as well as the spin levels of the ground state from which these start enables us to construct the energy level diagram, and the result is given in Fig. 14.

The ground-state level splittings, which now have been determined from the line *positions* [for instance from the Landé sequence of the lines 6960 Å-6976 Å-N_3-N_4 (see Fig. 14)] can be described by

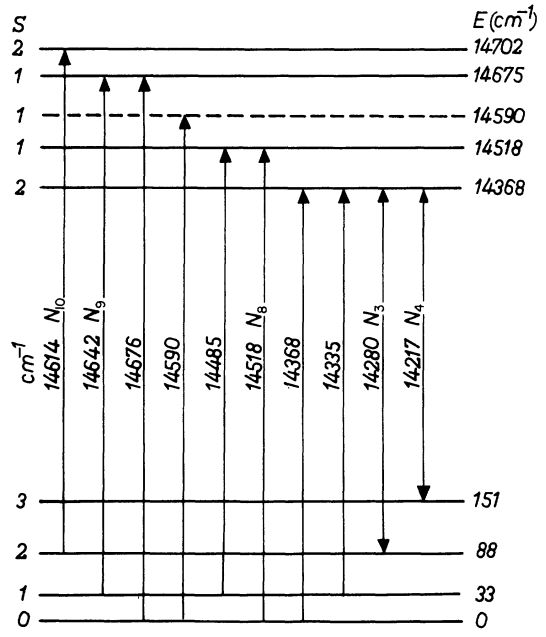

FIG. 14. Energy-level diagram of the nearest-neighbor Cr^{3+} pairs as determined from the experimental results.

the exchange Hamiltonian (1) with

$$J=(-22.2\pm0.5)\ \text{cm}^{-1}\,,\quad j=(-1.7\pm0.3)\ \text{cm}^{-1}\,.$$

The agreement with the values found from the temperature dependence of the line intensities (Sec. IV B 2) is very good.

It is of great importance to deduce which value of S ($S=1$ or $S=2$) belongs to each level of the excited state. Since we are not able to find this in a direct way (for instance, via Zeeman effect measurements), we will try to deduce this with the help of some theoretical considerations. As pointed out in Sec. III C, there are two additive mechanisms which induce the optical transitions. The exchange-induced dipole moment gives rise to $\Delta S=0$ transitions while magnetic dipole transitions have $\Delta S=0,\ \pm1$. It has been found in comparable cases[27,41,43] that the strongest lines in the nn pair spectrum are e.i.d. transitions. Therefore, it is reasonable to assume that the strongest lines, N_3, N_9, and N_{10}, are $\Delta S=0$ transitions. Transitions from the $S=0$ ground-state level must be m.d. [the oscillator strengths of these lines are indeed close to the values of the R lines (Table IV)] and the excited-state levels on which they end will be $S=1$ levels. $\Delta S=2$ transitions must be much weaker. Using these rules, the spin values of the excited-state levels have been determined and are given in Fig. 14. The $S=2$ assignment of the 14702-cm^{-1} level is, perhaps, open to some doubt, because only one transition (N_{10}) to this level has been identified.

We observe that N_4 is remarkable strong (Fig. 5 and Table IV). Since N_4 starts (or ends) on the $S=3$ ground-state level, it must be a m.d. transition. It is found that N_4 is stronger than the other $\Delta S=\pm1$ lines. The same situation occurs in the case $LaAlO_3:Cr^{3+}$.[27] We believe that this is caused by the high spin degeneracy of the $S=3$ level which may lead to a large m.d. transition probability (see also the calculations of Pryce[26]). Finally, we remark that the $S=2$ assignment of the lowest excited state level (Fig. 14) is strongly supported by the fact that N_4 is so strong. If this level had $S=1$, N_4 should be much weaker and the line at 6976 Å much stronger.

V. COMPARISON OF THEORY AND EXPERIMENT

In Sec. IV we have found that the ground-state ($^4A_2$, $^4A_2$) level splittings could be described by the exchange Hamiltonian (1), with $J=(-22.2\pm0.5)$ cm^{-1} and $j=(1.7\pm0.3)$ cm^{-1}.

The analysis of the excited- ($^4A_2$, ^2E) state level splittings is more difficult because now we have to find *four* exchange parameters (J_c, J_c', J_d, and J_r) by fitting the observed level structure of the ($^4A_2$, ^2E) state (Fig. 14) to the theoretical energy-level scheme (Table I). The fitting procedure is complicated by the fact that, in general, the $^2E-{}^4A_2$ energy difference (denoted by E_0 in Sec. III) is not equal to the E_0 value of the single ions (usually called R, which amounts to 14570 cm^{-1}), for several reasons; (i) A slightly different crystal field is seen by a Cr^{3+} ion when there is another Cr^{3+} ion as neighbor instead of Ga^{3+}. (ii) Exchange interactions of the ($^4A_2$, ^2E) state with other pair states [e.g., ($^4A_2$, $^4A_2$) or ($^4A_2$, $^2T_1$)] may cause, in second-order perturbation theory, a small shift of the ($^4A_2$, ^2E) levels as a whole [and, of course, shifts of the ($^4A_2$, ^2E) levels relative to each other]. Therefore, we shall assume that the precise value of E_0 is unknown but it will not differ much from $R=14\,570$ cm^{-1}.

In Sec. IV it was found that the lowest excited-state level has total spin $S=2$. In Sec. VI it is argued that J_c and J_c' are positive and that J_d and J_r are negative. Hence, recalling the definitions in (11) we have

$$N>0\,,\quad N>|K|,|L|\,. \tag{30}$$

It can then be shown that the lowest excited-state level is either $^5\Gamma_3$ or $^5\Gamma_2$.

First we use only the four levels which have been established with certainty, namely the levels at 14 368 cm^{-1}, 14 518 cm^{-1}, 14 675 cm^{-1}, and 14 702 cm^{-1} (Fig. 14). Clearly, it is impossible to derive the four exchange parameters and E_0 from these four level positions and therefore we shall assume $E_0=R=14\,570$ cm^{-1}. Further, in order to compare with theory, we should remember that,

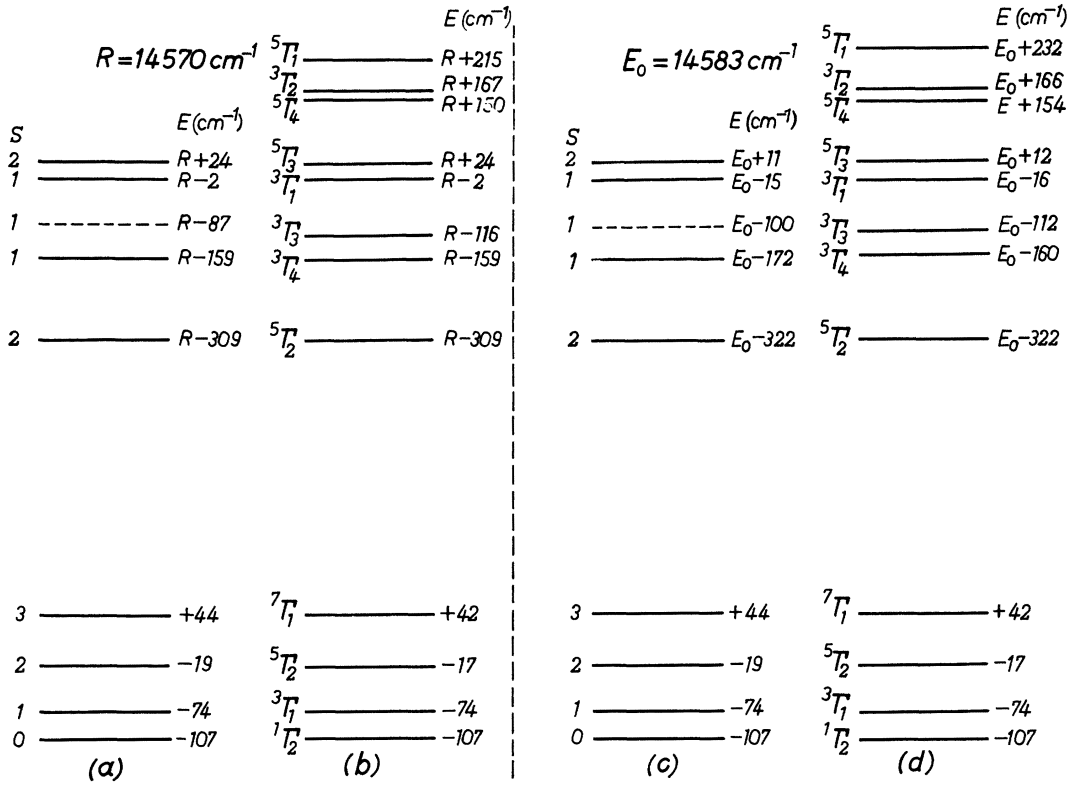

FIG. 15. (a) and (c) Experimental energy-level scheme. (b) Theoretical energy-level scheme calculated from Eq. (2) and Table I using, for the ground state, $J=-22.2$ cm^{-1}, $j=-1.7$ cm^{-1} and for the excited state, $N=+53$ cm^{-1}, $K=+33$ cm cm^{-1}, $L=+22$ cm^{-1}, $J=-22$ cm^{-1}. (d) Theoretical energy-level scheme calculated with the same ground-state parameters as in (b) and for the excited state: $N=+58$ cm^{-1}, $K=+34$ cm^{-1}, $L=+21$ cm^{-1}, and $J=-25$ cm^{-1}.

in the calculation of the energy levels of the pair, the zero of energy is chosen as the ground state of the single ions (or, equivalently, the imaginary ground state of the pairs without exchange coupling). So, the $\frac{15}{4}J+\frac{225}{16}j$ [see (2), which amounts to -107 cm^{-1}] depression of the $S=0$ level has to be accounted for. At first, we tried to fit the theoretical levels to the experimental ones, assuming $^5\Gamma_3$ lowest and using the constraints of Eq. (30). It was found that such a fit is not possible. Assuming $^5\Gamma_2$ lowest, it turned out that there was only one solution which gave a reasonable fit, the assignment of the levels is $^5\Gamma_2$ at $R-309$ cm^{-1}, $^3\Gamma_4$ at $R-159$ cm^{-1}, $^3\Gamma_1$ at $R-2$ cm^{-1}, and $^5\Gamma_3$ at $R+24$ cm^{-1} [see Figs. 15(a) and 15(b)]. The N, K, L, J are determined as

$$N=+53\text{ cm}^{-1},\quad K=+33\text{ cm}^{-1},\quad L=+22\text{ cm}^{-1},\quad J=-22\text{ cm}^{-1}, \tag{31a}$$

which gives, using Eq. (14),

$$J_c=+44\text{ cm}^{-1},\quad J_c'=+104\text{ cm}^{-1},\quad J_d=-542\text{ cm}^{-1},\quad J_\tau=-83\text{ cm}^{-1}. \tag{31b}$$

The $^3\Gamma_3$ level is then calculated at $R-116$ cm^{-1}. Experimentally, such a level is not found but it strongly suggests that the (uncertain) $R-87$ cm^{-1} level [Figs. 15(a) and 15(b)] should be identified with this $^3\Gamma_3$ level. Now, accepting the $R-87$ cm^{-1} level as a n.n. pair level, we have made the best over-all fit to all five levels (without the assumption $E_0=R$) which is obtained for

$$N=+58\text{ cm}^{-1},\quad K=+34\text{ cm}^{-1},\quad L=+21\text{ cm}^{-1},\quad J=-25\text{ cm}^{-1},\quad E_0=14\,583\text{ cm}^{-1}, \tag{32a}$$

which leads to

$$J_c=+39\text{ cm}^{-1},\quad J_c'=+117\text{ cm}^{-1},\quad J_d=-561\text{ cm}^{-1},\quad J_\tau=-105\text{ cm}^{-1}. \tag{32b}$$

This is represented in Figs. 15(c) and 15(d). It is seen that all five levels are reproduced within 12 cm^{-1}. In view of the experimental inaccuracies, the theoretical uncertainties (the neglect of biquadratic exchange in the excited state) and comparing (31) with (32), we estimate the relative accuracy of the determined values of the exchange parameters to be 10–20%. It is very satisfactory that the value of J as extracted from the excited-state level splittings is close to the value found from

the analysis of the ground state. The difference $E_0 - R$ amounts to 13 cm^{-1}, which would mean that the $^2E - {}^4A_2$ energy difference of nn pairs is 0.09% larger than the single-ion value, which seems to be an acceptable value.

The intensities of the different pair lines are of considerable interest and in the following the experimental values (Table IV) and the theoretical values (Table II) will be compared. First we look at the intensities of N_3 and N_9 which are, respectively, $AA^5\Gamma_2 \rightarrow AE^5\Gamma_2$ and $AA^3\Gamma_1 \rightarrow AE^3\Gamma_1$ transitions. From Table II it can be seen that the expected ratio is 1.8. Experimentally we measure, of course, the sum of the e.i.d. and m.d. transition probabilities, but making the crude approximation of neglecting the m.d. intensity then the experimental ratio of 1.5 is in reasonable agreement with the theoretical ratio. If we do the same for the line N_{10} ($AA^5\Gamma_2 \rightarrow AE^5\Gamma_3$) and the line at 6904 Å ($AA^3\Gamma_1 \rightarrow AE^3\Gamma_4$), we find a ratio of 1.7, the predicted ratio again being 1.8. This may serve as a check that the assignments of the levels, as given above, are correct.

We remark that we have not been able to find the three remaining levels, $AE^3\Gamma_2$, $AE^5\Gamma_4$, and $AE^5\Gamma_1$. Transitions to these levels are expected to occur in regions with strong R line vibronics which make the observation difficult. From Table II it can be seen that the e.i.d. transition probabilities for $AE^5\Gamma_4$ is zero and for $AE^5\Gamma_1$ and $^3\Gamma_2$ determined by P_2 and P_3. It is possible that P_2 and P_3 are smaller than P_1 and P_4, which also would cause the nonobservation of these levels.

Finally, we recall that in Sec. IV B it was found that N_3 has very strong vibronics. A possible explanation for this will be given in the Appendix.

VI. DISCUSSION

A. Optical Ground State

From the level splittings of the ($^4A_2$, $^4A_2$) state we found for the isotropic bilinear an biquadratic exchange parameters of nn Cr^{3+} pairs: $J = -22.2$ cm^{-1} and $j = -1.7$ cm^{-1}, respectively. This is in good agreement with the results of the ESR measurements.[19] The negative value of J, indicating an antiferromagnetic coupling of the ionic spins, is to be expected, since the asymptotic Curie temperature Θ_C of the concentrated material is negative ($\Theta_C = -330$ °K[45]). The contribution of the nn pair interaction to the asymptotic Curie temperature can be found from

$$\Theta_C(\text{nn pairs}) = [2S(S+1)/k]\, J_{nn}, \qquad (33)$$

where $S = \frac{3}{2}$; we find that Θ_C (nn pairs) $= -240$ °K. The difference Θ_C(total) $- \Theta_C$(n.n. pairs) is apparently caused by non-nearest-neighbor interactions.

The large value of j (this means large relative to J) can be explained on the basis of an exchange striction model.[18,19]

B. Orbital Exchange Parameters

Exchange processes can be divided into two main categories, potential and kinetic exchange.[46]

(i) *Potential exchange.* This type of exchange originates from the electrostatic repulsion between electrons, together with the Pauli exclusion principle. This type of interaction was considered by Heisenberg as early as 1926; it always gives rise to ferromagnetic coupling.

(ii) *Kinetic exchange.* This type of exchange, proposed by Anderson[10,46] and by Yamashita and Kondo[47] is based on the fact that the kinetic energy of the pair system is lowered when electron transfer takes place between orbitals of the different ions. This may be either direct cation → cation transfer, in which case the orbitals of the electrons which are transferred must have an appreciable overlap with each other, or indirect cation → anion → cation transfer, which is possible if the orbitals have nonzero overlap with one intermediate oxygen orbital. Anderson[10,46] has shown that the kinetic exchange, if allowed, dominates the potential exchange. This is in agreement with the empirical fact that almost all magnetic insulators are antiferromagnets. It can easily be seen that the orbitals ζ_A and ζ_B (A and B denote Cr^{3+} ion A and B, respectively) have nonzero overlap with each other; the orbitals ξ_A and η_B both overlap with an oxygen P_z orbital. The exchange interactions between ξ_A and ξ_B and between ξ_A and ζ_B are governed by the potential exchange process. Therefore it seems reasonable to assume that $J_{\xi\xi} = J_d$ and $J_{\xi\eta} = J_\pi$ are negative and $J_{\xi\zeta} = J_c$ and $J_{\zeta\zeta} = J_c'$ are positive.

In Sec. V we found $J_c = +39$, $J_c' = +117$, $J_d = -561$, and $J_\pi = -105$ cm^{-1}. Analysis of these figures would entail extensive and tedious calculations which is beyond the scope of this paper. However, one of the important conclusions that can be drawn is that our measurements, i.e., the determined value $J_d = -561$ cm^{-1}, support the model explaining the dependence of the asymptotic Curie temperature on the Cr^{3+}-Cr^{3+} distance, as has been put forward in the introduction.

The value of J, which is related to the J_{ij} parameters through Eq. (5), as found for the ($^4A_2$, ^2E) state is close to the J value found for the ground state. This, in turn, indicates that the J_{ij}'s of the ground state will not differ much from those of the excited state (if the t_{2g} orbitals of the ground state and optical exicted state are exactly the same, then they will be identical).

The values of the J_{ij}'s as determined by us, may be a help in the general understanding of the

exchange processes which are important in compounds with a 90° exchange configuration. This demonstrates the power of the optical measuring method which provides us detailed information which cannot be obtained from measurements of the $({}^4A_2, {}^4A_2)$ state alone.

ACKNOWLEDGMENTS

The authors are grateful to Professor M. H. L. Pryce for a preprint of his paper on exchange-coupled Cr^{3+} pairs in ruby. We are also indebted to J. P. M. Damen for growing the single crystals, to A. B. Voermans for preparing the powder samples, to L. C. Bastings for the chemical analyses, to A. T. Vink and A. Bril for measuring facilities, to J. A. de Poorter for performing some of the decay-time measurements, and to A. H. M. Crone and R. L. A. v. d. Heijden for technical assistance.

APPENDIX: EXCHANGE-INDUCED DIPOLE MOMENT

Electric dipole moment transition probabilities are proportional to the square of the matrix elements of the electric dipole operator $\vec{P} = \sum_i e\vec{r}_i$ (i runs over the six t_{2g} electrons):

$$\langle AA^{2S+1}\Gamma | \vec{P} | AE^{2S+1}\Gamma' \rangle . \qquad \text{(A1)}$$

In lowest-order perturbation theory (A1) equals zero, of course, but the exchange interaction between the electrons of ion A and those of ion B mixes odd-parity states in the wave functions, making (A1) nonzero. It seems that several mechanisms are operative at the same time.[33] As an example

$$\langle \varphi_{iA}\bar{\varphi}_{jB} | \vec{P}_{ex,ij} | \varphi_{jB}\bar{\varphi}_{iA} \rangle = \sum_\mu \frac{1}{E(\varphi_\mu) - E(\varphi_i)} \times \langle \varphi_{iA}\bar{\varphi}_{jB} | \vec{P} | \varphi_{\mu A}\bar{\varphi}_{jB} \rangle \langle \varphi_{\mu A}\bar{\varphi}_{jB} | V | \varphi_{jB}\bar{\varphi}_{iA} \rangle + \sum_\nu \frac{1}{E(\varphi_\nu) - E(\varphi_j)} \langle \varphi_{iA}\bar{\varphi}_{jB} | \vec{P} | \varphi_{iA}\bar{\varphi}_{\nu B} \rangle \times \langle \varphi_{iA}\bar{\varphi}_{\nu B} | V | \varphi_{jB}\bar{\varphi}_{iA} \rangle , \qquad \text{(A2)}$$

where φ_{iA} and $\bar{\varphi}_{jB}$ are t_{2g} wave functions of an electron with spin up in orbital i on A and an electron with spin down in orbital j on ion B, respectively; $V = r_{12}^{-1}$ is the two-electron Coulomb operator; and $\varphi_{\mu A}$, $\varphi_{\nu B}$ are wave functions of odd-parity orbitals on ion A and ion B, respectively.

Another mechanism, closely related to the superexchange mechanism, can be written

$$\langle \varphi_{iA}\bar{\varphi}_{jB} | \vec{P}_{ex,ij} | \varphi_{jB}\bar{\varphi}_{iA} \rangle = \frac{1}{U} \sum_\mu \frac{1}{E(\varphi_\mu) - E(\varphi_i)} \times \langle \varphi_{iA}\bar{\varphi}_{jB} | \vec{P} | \varphi_{\mu A}\bar{\varphi}_{jB} \rangle \langle \varphi_{\mu A}\bar{\varphi}_{jB} | \nabla^2 | \varphi_{jB}\bar{\varphi}_{jB} \rangle \times \langle \varphi_{jB}\bar{\varphi}_{jB} | \nabla^2 | \varphi_{jB}\bar{\varphi}_{iA} \rangle + \frac{1}{U} \sum_\nu \frac{1}{E(\varphi_\nu) - E(\varphi_j)} \times \langle \varphi_{iA}\bar{\varphi}_{jB} | \vec{P} | \varphi_{iA}\bar{\varphi}_{\nu B} \rangle \langle \varphi_{iA}\bar{\varphi}_{\nu B} | \nabla^2 | \varphi_{iA}\bar{\varphi}_{iA} \rangle \times \langle \varphi_{iA}\bar{\varphi}_{iA} | \nabla^2 | \varphi_{jB}\bar{\varphi}_{iA} \rangle , \qquad \text{(A3)}$$

where $U = E(\varphi_{1A}, \bar{\varphi}_{2B}) - E(\varphi_{1B}, \bar{\varphi}_{2B})$ is the energy difference between states where the t_{2g} electrons are on different ions and the same, respectively, and ∇^2 is the kinetic energy operator.

By using spin operators $\vec{s}_{iA}$ and $\vec{s}_{jB}$ the operator equivalent of Eqs. (A2) and (A3) may be expressed as

$$\vec{P}_{ex,ij} = \vec{P}_{ij}\, \vec{s}_{iA} \cdot \vec{s}_{jB} , \qquad \text{(A4)}$$

and summing over all six electrons leads to Eq. (16).

Clearly, it is extremely difficult to evaluate expressions like (A2) and (A3) to get numerical estimates of the $\vec{P}_{ij}$'s. Therefore, the $\vec{P}_{ij}$'s are treated as empirical parameters, the values of which may be determined from the experiments.

Finally, we would like to give a possible explanation of the experimental fact that the n n pair line N_3 has very strong vibronics, while N_4 has not (see Fig. 5). As has been shown in Sec. V, N_3 is the transition $AA\,{}^5\Gamma_2 \leftarrow\!\!\!\rightarrow AE\,{}^5\Gamma_2$, with a transition probability proportional to the square of $P_4 = -P^x_{\xi\xi} + P^x_{\zeta\zeta} + P^x_{\zeta\zeta} + P^x_{\xi\eta}$. It can be shown that if the trigonal field at the Cr^{3+} ions would be absent (which would raise the pair symmetry to D_{2h} and lead to pure t_{2g} orbitals), then all P^x_{ij} would be zero. Apparently, in that case, the sum over all terms of (A2) and (A3) is precisely zero, while the individual terms of (A2) and (A3) may be nonzero. The fact that the orbitals are not pure t_{2g} (through the action of the trigonal field) makes P_4 nonzero and this gives rise to the zero-phonon line N_3. The vibronic interaction, also destroying the pure t_{2g} character of the wave functions, induces the phonon sidebands of N_3. Since N_4 is not an e.i.d. transition, this mechanism is not operative for N_4 and therefore the intensity of the vibronic sidebands of N_4 relative to N_4 is similar to that of the sidebands of the R lines relative to the R lines.

[1] P. F. Bongers, dissertation (University of Leiden, 1957) (unpublished).

[2] W. Rüdorff and K. Stegemann, Z. Anorg. Allg. Chem. **251**, 376 (1943).

[3] F. K. Lotgering, in *Proceedings of the International Conference on Magnetism, Nottingham, England, 1964* (The Institute of Physics and the Physical Society, London, 1965), p. 533.

[4] P. K. Baltzer, P. J. Wojtowicz, M. Robbins, and E. Lopatin, Phys. Rev. **151**, 367 (1966).

[5] N. Menyuk, K. Dwight, J. Arnott, and A. Wold, J. Appl. Phys. **37**, 1387 (1966).

[6]P. F. Bongers and E. R. van Meurs, J. Appl. Phys. **38**, 944 (1967).
[7]P. K. Baltzer, H. W. Lehmann, and M. Robbins, Phys. Rev. Lett. **15**, 493 (1965).
[8]J. Kanamori, J. Phys. Chem. Solids **10**, 87 (1959).
[9]J. B. Goodenough, Phys. Rev. **100**, 564 (1955).
[10]P. W. Anderson, Phys. Rev. **115**, 2 (1959).
[11]E. O. Wollan, Phys. Rev. **117**, 387 (1960).
[12]J. B. Goodenough, Phys. Rev. **117**, 1442 (1960).
[13]K. W. Blazey, Solid State Commun. **4**, 541 (1966).
[14]D. L. Wood, G. F. Imbusch, R. M. Macfarlane, P. Kisliuk, and D. M. Larkin, J. Chem. Phys. **48**, 5255 (1968).
[15]K. Motida and S. Miyahara, J. Phys. Soc. Jap. **28**, 1188 (1970); J. Phys. Soc. Jap. **29**, 516 (1970).
[16]J. Hornstra and E. Keulen, Philips Res. Rep. **27**, 76 (1972).
[17]J. C. M. Henning, Phys. Lett. **34**, 215 (1971).
[18]J. C. M. Henning and J. P. M. Damen, Phys. Rev. B **3**, 3852 (1971).
[19]J. C. M. Henning, J. H. den Boef, and G. G. P. van Gorkom, Phys. Rev. B **7**, 1825 (1973).
[20]H. van den Boom, J. C. M. Henning, and J. P. M. Damen, Solid State Commun. **8**, 717 (1970).
[21]A. M. Clogston (unpublished).
[22]A. E. Nikiforov and V. I. Cherepanov, Phys. Status Solidi **14**, 391 (1966).
[23]J. H. Van Vleck, Rev. Mat. Fis. Teor. Univ. Nac. Tucuman **14**, 189 (1962).
[24]R. J. Elliott and M. F. Thorpe, J. Appl. Phys. **39**, 802 (1968).
[25]J. W. Culvahouse and D. P. Schinke, Phys. Rev. **187**, 671 (1969).
[26]M. H. L. Pryce (unpublished).
[27]J. P. van der Ziel, Phys. Rev. B **4**, 2888 (1971).
[28]N. L. Huang, Phys. Rev. B **1**, 945 (1970).
[29]R. J. Birgeneau, J. Chem. Phys. **50**, 4282 (1969).
[30]See, e.g., V. Heine, *Group Theory in Quantum Mechanics* (Pergamon, Oxford, 1966).
[31]G. F. Koster, J. O. Dimmock, R. G. Wheeler, and H. Statz, *Properties of the Thirty-Two Point Groups* (MIT Press, Cambridge, Mass., 1963).
[32]S. Sugano and Y. Tanabe, J. Phys. Soc. Jap. **13**, 880 (1958).
[33]Y. Tanabe, T. Moriya, and S. Sugano, Phys. Rev. Lett. **15**, 1023 (1965); K. I. Gondaira and Y. Tanabe, J. Phys. Soc. Jap. **21**, 1527 (1966).
[34]H. M. Kahan and R. M. Macfarlane, J. Chem. Phys. **54**, 5197 (1971).
[35]J. Preudhomme and P. Tarte, Spectrochim. Acta A **27**, 1817 (1971).
[36]G. G. P. van Gorkom and J. H. Haanstra (unpublished).
[37]S. Sugano, A. Schawlow, and F. Varsanyi, Phys. Rev. **120**, 2045 (1960).
[38]G. F. Imbusch, Ph.D. thesis (Stanford University, 1964) (unpublished).
[39]An excellent description of energy transfer effects (in ruby) has been given by G. F. Imbusch [Phys. Rev. **153**, 326 (1967)].
[40]S. K. Lyo, Phys. Rev. B **3**, 3331 (1971).
[41]M. J. Berggren, G. F. Imbusch, and P. L. Scott, Phys. Rev. **188**, 675 (1969).
[42]J. Heber, K. H. Hellwege, S. Leutloff, and W. Platz, Z. Phys. **246**, 261 (1971).
[43]P. Kisliuk, N. C. Chang, and M. H. L. Pryce, Phys. Rev. **184**, 367 (1969).
[44]J. P. van den Ziel, J. Chem. Phys. **57**, 2442 (1972).
[45]Y. Kino and B. Lüthi, Solid State Commun. **9**, 805 (1971).
[46]P. W. Anderson, in *Magnetism*, edited by G. T. Rado and H. Suhl (Academic, New York, 1963).
[47]J. Yamashita and J. Kondo, Phys. Rev. **109**, 730 (1958).

PHYSICAL REVIEW B VOLUME 8, NUMBER 3 1 AUGUST 1973

NMR Studies of Dilute Alloys of Ni in Cu†

David C. Lo,* David V. Lang,‡ James B. Boyce, and Charles P. Slichter
Department of Physics and Materials Research Laboratory, University of Illinois, Urbana, Illinois 61801
(Received 29 December 1972)

We have studied the nuclear magnetic resonance of Cu atoms which are near neighbors to Ni atoms in dilute *Cu* Ni alloys. The experiments were performed at liquid-helium temperatures and at magnetic fields from 6 to 60 kG. The resonances show up as weak satellites to the main absorption of more distant Cu. By varying the magnetic field, we can show that several lines arise from a single shell of neighbors having a quadrupole coupling $\nu_q = 1.1 \pm 0.1$ MHz, asymmetry parameter $\eta = 0.20 \pm 0.05$, and a magnetic shift $\Delta H/H = -0.27 \times 10^{-3}$. Comparing the quadrupole coupling with estimates made by Béal-Monod and Tompa for CuNi by measuring wipe-out number, we conclude the lines arise from first neighbors. The magnetic shift is smaller than we had previously observed for CuCo in almost exactly the ratio of the χJ's of the two impurities, where χ is the impurity susceptibility and J is the *s-d* exchange coupling.

I. INTRODUCTION

Over the past several years there has been extensive interest in the occurrence or lack of occurrence of magnetization when transition-metal atoms are present at low concentration in nonmagnetic hosts such as copper or gold. These are systems in which the Kondo effect is often observed. For the Kondo effect it is thought that at low temperatures the conduction electrons pair up with the spin of the impurities to form a many-body singlet. One of the most powerful techniques for study of these systems has been nuclear magnetic resonance. Heeger and his collaborators through a series of papers[1] have studied the broadening of the resonance of the host copper produced by the magnetic atoms especially for the system copper containing iron. Potts and Welsh[2] have extended these data.